Doklady Physics, Vol. 45, No. 3, 2000, pp. 101–104. Translated from Doklady Akademii Nauk, Vol. 371, No. 1, 2000, pp. 45–48.

TECHNICAL PHYSICS

Twinning in Gadfield-Steel Single Crystals

Yu. I. Chumlyakov*, I. V. Kireeva*, E. I. Litvinova*, E. G. Zakharova*, N. V. Luzginova*, Corresponding member of the RAS S. P. Efimenko, H. Seĭhitoglu***, and I. Karaman*****

Received October 14, 1999

Mechanical twinning in Gadfield-steel polycrystals (containing 12 wt % of Mn and 1 wt % of C, in addition to Fe) promotes the high rate Θ of strain hardening [1–6]. The combined effect of a high concentration of interstitial atoms C_C = 1–1.3% and the low energy of stacking faults γ_{sf} = 0.025 J/m^2 gives rise to the fact that we can observe twinning within a wide temperature range after a small strain by slipping in the case of both tension and compression [1–3]. Hence, the interstitials introduced into the fcc host do not suppress twinning, although the $a/6\langle 211\rangle$ shear by twinning removes carbon atoms from octahedral interstitial positions to tetrahedral ones. On the contrary, the interstitials stimulate intense twinning [1–3]. The twins induced by strains in Gadfield steel are, in fact, pseudotwins, since positions of interstitial atoms in the untwinned material and in the twin turn out to be nonequivalent [1, 7, 8]. Therefore, the pseudotwins are more efficient obstacles to slipping and twinning in intersecting systems compared to twins in pure fcc metals and substitution alloys [7]. The high rate of strain hardening in Gadfield steel can be explained on the basis of this concept [1].

A widespread interest in mechanical twinning in Gadfield-steel single crystals is associated, first of all, with the fact that only single crystals allow us to reveal basic regularities in the orientation dependence of twinning [4–6]. According to previous experimental data for fcc crystals [7], it is possible to vary the multiplicity of the twin-induced shear by changing orientation of the tension axis in a crystal. For $[\bar{1}11]$ orientations, three intersecting systems of twins have the same Schmid factors, whereas for $[\bar{1}44]$ and $[\bar{3}77]$ orientations, there exists only one such a system. For [001] orientations, deformation could occur only by slipping, since twinning was not observed previously in fcc crystals for these orientations [7]. The second source of interest is related to features of twinning. Twinning accompanying the $[\bar{1}11]$ tension of crystals should be generated by $a/6[\bar{2}11]$ (111) dislocations in the primary slipping system, whereas the reverse twin-induced $a/6[2\bar{1}\bar{1}]$ shear was not observed in experiments in which compression of these crystals was used. This shear causes formation of *AA* stacking in the three-layer model of the fcc lattice [7, 10]. Therefore, the formation of such high-energy defects requires higher stresses compared to those characteristic of the competing (namely, slipping) strain mechanism. Another possibility for the strain by twinning in the course of the compression of $[\bar{1}11]$ crystals is related to formation of two-layer extrinsic stacking faults [10]. In this case, the $a/6[2\bar{1}\bar{1}]$ shear can be represented as a sum of two shears in the *AA* plane ($a/6[1\bar{2}1]$) and in the neighboring plane above *A* ($a/6[11\bar{2}]$). Although the energy γ_e of extrinsic stacking faults exceeds only slightly that of intrinsic stacking faults γ_I, the former are observed in experiments much more rarely than the latter ones and do not play an equally important role in the mechanical twinning [7, 10]. The goal of the present paper is the experimental study of the orientation dependence of strain by twinning in the case of strain by tension or compression, and to reveal a possibility of twinning owing to the motion of extrinsic stacking faults.

The Gadfield-steel single crystals were produced by the Bridgman method, i.e., by seeded growth in the rare-gas ambient. The sample preparation and experimental technique are reported in detail in [5, 6].

It was demonstrated experimentally that in the case of tension of $[\bar{1}11]$, $[\bar{1}44]$, $[\bar{3}77]$ and [011] crystals, the strain by twinning is observed from the very beginning of the plastic deformation (see Fig. 1, curves *1*, *2*, and *3*). The twins are easily revealed by the metallographic technique, electron microscopy, and X-ray diffraction

* *Siberian Institute of Physics and Technology, Tomsk State University, Novosobornaya pl. 1, Tomsk, 634050 Russia*

** *Baikov Institute of Metallurgy, Russian Academy of Sciences, Leninskiĭ pr. 49, Moscow, 117911 Russia*

*** *144 Mechanical Engineering Building, University of Illinois at Urbana–Champaign, 1206 West Green Street, Urbana, Illinois, 61801 USA*

1028-3358/00/4503-0101$20.00

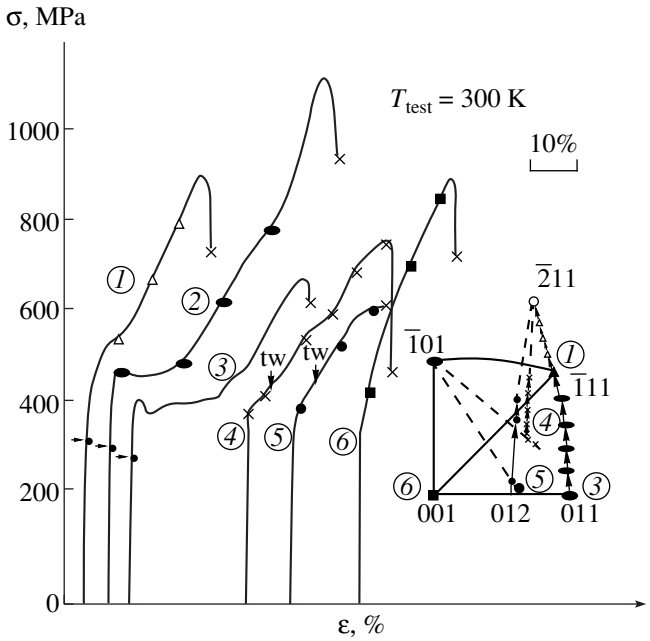

Fig. 1. Flow curves for the Gadfield-steel single crystals in the case of tension: (*1*) [$\bar{1}$11]; (*2*) [$\bar{3}$77]; (*3*) [011]; (*4*) [$\bar{1}$23]; (*5*) [012]; (*6*) [011]. Numbers in circles denote both the flow curves and the crystal-axis precession corresponding to these curves.

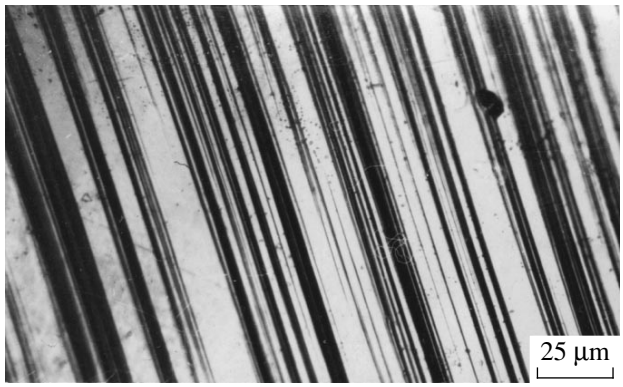

Fig. 2. Twinning by a Luders band in the case of tension of [$\bar{3}$77] crystals. ε = 6.4%, T_{test} = 300 K.

(Figs. 1–4). In the [$\bar{1}$11] crystals, the high values of Θ are related to the development of twinning in two intersecting systems. In this case, one of the twinning systems turns out to be more developed than the other. The precession of the crystal axis demonstrates that the orientation of the sample axis varies along a large circle passing through the [$\bar{1}$11]–[011] poles in the [$\bar{2}$11] direction (Fig. 1). Theoretical estimates of the crystal-axis position, which were obtained under assumption that only one twinning system is efficient, exceed only slightly the measured values. It is clear that this difference stems from the activation of secondary twinning systems. Their interaction with the primary one gives rise to high values of Θ and determines the linearity of the dependence σ(ε) [5, 6].

Metallographic studies of [$\bar{1}$44], [$\bar{3}$77] and [011] crystals demonstrate that twining develops there through the Luders band in the single twinning system [$\bar{2}$11] (111) from the very beginning of the plastic flow (Fig. 1, curves *2*, *3* and Fig. 2). This stage of deformation corresponds to the portion of the flow curve with the strain-hardening coefficient Θ close to zero. The passage to the stage with high Θ correlates with the formation of the secondary twinning systems. Thus, for the development of strains by twinning at the very beginning of the plastic flow in the Gadfield-steel crystals, the following conditions should be met. First, the Schmid factor for twinning m_{tw} should be larger than the corresponding factor m_{sl} for slipping (see table). Second, the Schmid factor m_1 and hence, the applied external stresses acting onto the leading Shockley dislocation $\mathbf{b}_1$ causing twinning, should exceed those acting onto the trailing dislocation $\mathbf{b}_2$. Therefore, the Schmid factor m_2 should be smaller than m_1 (see table). In combination with strong friction forces existing in the Gadfield steel due to the high concentration of carbon atoms, these two conditions favor easy nucleation and propagation of twins in such high-strength crystals according to the slipping-source mechanism [2, 7, 9]. This mechanism does not require a considerable strain by slipping, which precedes that by twinning.

For the [012] and [$\bar{1}$23] orientations, the geometric conditions of twinning turn out to be less favorable than of slipping ($m_{tw}/m_{sl} < 1$), see table. The difference in the Schmid factors for $\mathbf{b}_1$ and $\mathbf{b}_2$ dislocations becomes significantly smaller compared to the orientations discussed above (see table). For these orientations, it was found that the deformation begins from slipping (Fig. 1, curves *4* and *5*). The shear develops within a single system; the precession of the crystal axis tends exactly to the [$\bar{1}$01] pole along the large circle passing through the [$\bar{1}$01] pole and the initial orientation of the crystals (Fig. 1). The passage to twinning occurs after a considerable strain by slipping. The strain corresponding to the nucleation of the first twinning lamellas is indicated by an arrow at the flow curves (Fig. 1, curves *4* and *5*). Furthermore, we observe the stage of strain hardening related to twinning–slipping and twinning–twinning interactions. The change of strain mechanism from slipping to twinning occurs when the crystal axis does not attain the [001]–[$\bar{1}$11] symmetry line.

Thus, in contrast to well-studied regularities of twinning in pure fcc metals and in the substitution solid solutions with values γ_{sf} = 0.025–0.03 J/m^2, which are close to those in the Gadfield steel, the Gadfield-steel crystals exhibit certain qualitatively new features of

twinning. Indeed, in the former two materials, twinning is always preceded by slipping and, in the beginning of the twinning process, the crystal axis is located symmetrically [7]. Firstly, for $[\bar{1}11]$, [011], $[\bar{1}44]$, and $[\bar{3}77]$ orientations, twinning develops from the very beginning of the plastic flow without the macroscopic strain by slipping preceding twinning. Secondly, for [012] and $[\bar{1}23]$ orientations, twinning is preceded by slipping, and the passage to twinning is observed when the crystal axis does not become symmetrical. The energy of stacking faults is the same both in the Gadfield steel and in fcc crystals subjected to twinning. Therefore, the physical mechanisms of such a difference in the features of twinning cannot be related to the value of the energy γ_I. The difference is determined by different levels of the frictional distorting stresses [4–7]. The solid-solution hardening of the Gadfield steel by carbon, gives rise to the significant enhancement of the friction forces compared to Ag and Au crystals and copper-based alloys with the similar values of γ_I [7]. Thus, the necessary conditions for twinning in the Gadfield-steel crystals are met for the $[\bar{1}11]$ crystals owing to the non-dislocation hardening mechanism (the solid-solution hardening by interstitial atoms) rather than to usual strain hardening.

The importance of the high level of distorting strains for the development of twinning in the Gadfield-steel crystals manifests itself in the experimentally observed polarity phenomenon for the twinning shear in the case of the strain of $[\bar{1}11]$ crystals by tension or compression. For the compression of $[\bar{1}11]$ crystals, the strain by twinning is observed after a small stage of the unstable deformation associated with the formation of macroscopic shear bands. At the beginning of the plastic deformation, twinning develops in the two systems within the localized-shear bands, while at $\varepsilon > 9\%$, it is observed outside the regions of the localized strain (Fig. 3). The electron microscopy reveals the isolated stacking faults and thin microtwins (Fig. 4). Previously, twinning was not observed in the course of compression of $[\bar{1}11]$ crystals such as fcc metals and alloys. It is explained by the fact that the shear by twinning, which leads to intrinsic stacking faults in this orientation correspond to low values of the Schmid factor ($m_{tw} \sim 0.157$), which are much lower than those for slipping ($m_{sl} \sim 0.27$). In this case, twinning can be caused only by extrinsic stacking faults, and the Schmid factor for the $a/6[2\bar{1}\bar{1}]$ shear turns out to be high ($m_{tw} \sim 0.31$).

Therefore, in the high-strength Gadfield-steel crystals, twinning becomes the polar mechanism of the deformation in contrast to the features characteristic of twinning in the case of low-strength fcc crystals [7]. This conclusion is maintained by experimental observations of twinning accompanying tension of fcc crystals. Previously, mechanical twinning was not observed in experiments for fcc crystals of the [001] orientation

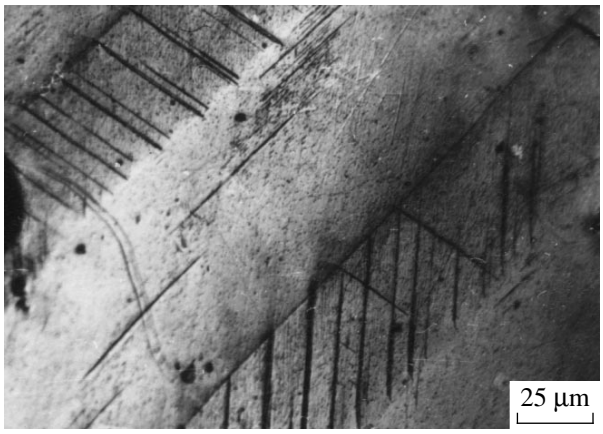

Fig. 3. Metallographic image of twinning in the case of compression of $[\bar{1}11]$ crystals. $\varepsilon = 9.8\%$, $T_{test} = 300$ K. The repeated polishing and etching were performed according to methods described in [1, 5, 6].

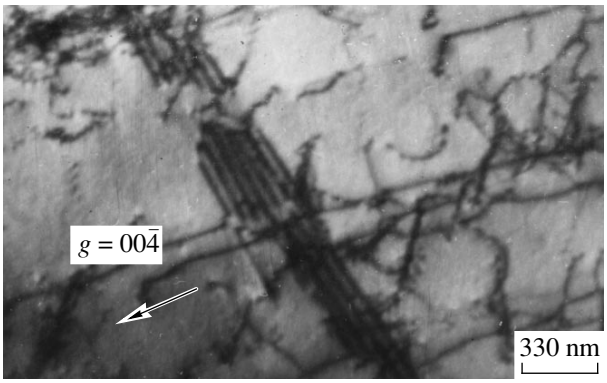

Fig. 4. Twinning in the case of compression of the $[\bar{1}11]$ crystals. $\varepsilon = 6\ \%$, $T_{test} = 300$ K.

Table 1. Schmid factors m_{sl} (for slipping) and m_{tw} (for twinning) and the factor $Q = (m_2 - m_1)/2$, where m_1 and m_2 are Schmid factors for the leading and trailing Shockley dislocations. (For orientations under study, these factors were determined in the case of tension at room temperature.)

Orientations	m_{sl}	m_{tw}	$Q = (m_2 - m_1)/2$
$\bar{1}11$	0.27	0.314	−0.08
$\bar{3}77$	0.40	0.50	−0.11
011	0.41	0.47	−0.12
$\bar{1}23$	0.45	0.45	−0.06
012	0.49	0.42	0
001	0.41	0.236	0.12

and for [$\bar{1}$11] crystals in the cases of strain by tension and compression, respectively. That is why these orientations were not considered as twinning orientations [7].

At the deformation by compression of [001] crystals, the twinning systems turn out to be more stressed than the slipping ones. The external-stress field favors splitting of a perfect dislocation into partial Shockley dislocations accompanying the formation of intrinsic stacking faults (see table). An intense twinning in the case of compression was observed for [001] crystals, which starts from early stages of plastic flow in the Gadfield-steel single crystals.

We may conclude that Gadfield-steel single crystals are characterized by the development of twinning from the beginning of the plastic flow without preceding slipping and by the polarity of the twin shear. These features are in a marked contrast with the behavior of pure fcc metals and substitution alloys. We can expect that similar features of the development of twinning could be found in single crystals of austenitic stainless steels characterized by low values of stacking fault energy $\gamma_{sf} = 0.020$ J/m^2, high nitrogen content $C_N >$ 0.5–0.7 wt %, and in the case of precipitation of nitrides.

ACKNOWLEDGMENTS

This work was supported by the Russian Ministry of Education (grant MATI-98 of the Moscow State University of Aviation Technology) and by the National Science Foundation (contract no. 94-14525)).

REFERENCES

1. P. H. Adler, G. B. Olson, and W. S. Owen, Met. Trans. A **17**, 1725 (1986).
2. K. S. Raghavan, A. S. Sastri, and M. J. Marcinkowski, Trans. TMS–AIME **245**, 1569 (1969).
3. Y. N. Dastur and W. C. Leslie, Met. Trans. A **12**, 749 (1981).
4. M. A. Shtremel' and I. A. Kovalenko, Fiz. Met. Metalloved. **63**, 172 (1987).
5. Yu. I. Chumlyakov, H. Seĭhitoglu, I. V. Kireeva, *et al.*, Dokl. Akad. Nauk **361**, 185 (1998) [Dokl. Phys. **43**, 415 (1998)].
6. I. Karaman, H. Seĭhitoglu, K. Gal, and Yu. I. Chumlyakov, Scripta Mater. **38**, 1009 (1998).
7. J. W. Christian and S. Mahajan, Prog. Met. Sci. **39**, 1 (1995).
8. J. W. Cahn, Acta Met. **25**, 1021 (1977).
9. S. M. Copley and B. H. Kear, Acta Met. **16**, 227 (1968).
10. J. P. Hirth and J. Lothe, *Theory of Dislocations*, 2nd ed. (Wiley, New York, 1982); 1st ed. (McGraw-Hill, New York, 1967; Moscow, Atomizdat, 1972).

Translated by K. Kugel'

Doklady Physics, Vol. 45, No. 3, 2000, pp. 105–107. Translated from Doklady Akademii Nauk, Vol. 371, No. 2, 2000, pp. 179–181.

TECHNICAL PHYSICS

Dependence of Elastic Properties of Microheterogeneous Polymeric Materials on Molecular and Structural Parameters

V. E. Zgaevskiĭ

Presented by Academician A.E. Shilov June 9, 1999

Received June 9, 1999

Certain materials, whose microscopic properties are functions of coordinates of their body points, are related to microheterogeneous polymeric materials. Their typical examples are cellulose, crystallizing rubbers, and, in part, crystalline polymers.

In this paper, the elastic mechanical properties of such materials are described within the framework of the scaling concept [1] with the use of the two-phase model. Basic structural and mechanical parameters are indicated, and the dependence of the elastic mechanical properties of such materials on these parameters are revealed.

On the basis of structural studies, it is established that the microheterogeneous polymeric materials, listed above, contain domains with the ordered arrangement of segments of extended polymeric macromolecules (crystallites) connected with each other by segments of chaotically tangled linking macromolecules (amorphous domains) [2–4]. At the next structural level, spatially alternating amorphous and crystalline regions give rise to fibrils from which the spherulites are formed. The fact that a spherulite is deformed under small elastic deformations, similar to the entire sample [5, 6], allows us to not consider it as a mechanically inhomogeneous formation. Thus, the isotropic materials indicated are modeled by chaotically oriented crystallites bound by segments of linking macromolecules (Fig. 1).

We consider an element of the model (bounded in Fig. 1 by solid lines), which incorporates a part of the crystallite with a segment of a macromolecule extending from it into an amorphous region. We will characterize the model element, the crystallite and the macromolecule segment in the amorphous domain, by vectors with components R_i^0, d_i^0, and l_i^0, respectively (Fig. 1). These components are connected by the relation

$$R_i^0 = d_i^0 + l_i^0. \quad (1)$$

Under the deformation of a model element, the vector components are transformed in the following manner:

$$\begin{aligned} R_i &= R_i^0 + X_{i,k}R_k^0, \\ d_i &= d_i^0 + \xi_{i,k}d_k^0, \\ l_i &= l_i^0 + \eta_{i,k}l_k^0, \end{aligned} \quad (2)$$

where the strain gradients for the model element, crystallite, and the macromolecule segment in the amorphous domain are denoted, respectively, by the expressions with indices separated by commas. Here and below, the summation is performed with respect to indices repeated twice. It follows immediately from relations (1) and (2) that

$$X_{i,k}R_k^0 = \xi_{i,k}d_k^0 + \eta_{i,k}l_k^0. \quad (3)$$

In accordance with the scaling representation, the free energy F_a of a macromolecule segment with the distance between the ends l and number of segment sections n is $F_a \sim \frac{3}{2}Tl^2n^{-1}a^{-2}$, where T is the absolute temperature in the energy units, and a is a linear size of the macromolecule segment section. We express l^2 in terms of the gradients $\eta_{i,k}$ [5]:

$$l^2 = l^{0^2} + (\eta_{l,i}\eta_{l,k} - \delta_{ik})l_i^0 l_k^0.$$

Using relation (3), we exclude gradient $\eta_{i,k}$ from l^2:

$$l^2 = X_{l,i}X_{l,k}R_k^0R_i^0 - 2X_{l,i}\xi_{l,k}R_i^0d_k^0 + \xi_{l,i}\xi_{l,k}d_i^0d_k^0. \quad (4)$$

The elastic energy of a crystallite in the approximation of an isotropic body [5] is

$$F_k \sim S^0d^0G\left(u_{ik}^2 + \frac{\nu}{1-2\nu}u_{ll}^2\right),$$

Institute of Chemical-Physics Problems, Russian Academy of Sciences, Chernogolovka, Moscow oblast, 142432 Russia

1028-3358/00/4503-0105$20.00

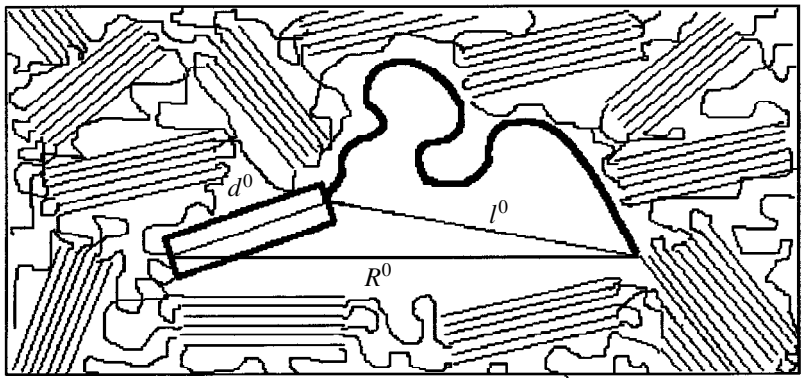

Model of a microheterogeneous polymeric material.

where S^0 is the area of the crystallite cross section perpendicular to the direction of the macromolecule and related to one macromolecule segment in the amorphous domain, G is the shear modulus, ν is the Poisson's ratio for a crystallite, u_{ik}^2 is the sum of squares for the components of the crystallite strain tensor $u_{ik} = \frac{1}{2}(\xi_{l,i}\xi_{l,k} - \delta_{ik})$, and u_{ll}^2 is the square of the sum of these components. Replacing the proportionality sign by the equality sign, as is often implied in the scaling theory, we write out the elastic energy of a model element as $F = F_a + F_k$. Then, we obtain on the basis of (4)

$$\begin{aligned} F = {} & \frac{3T}{2na^2}(X_{l,i}X_{l,k}R_i^0R_k^0 \\ & - 2X_{l,i}\xi_{l,k}R_i^0d_k^0 + \xi_{l,i}\xi_{l,k}d_i^0d_k^0) \\ & + S^0d^0G\left[\frac{1}{4}(\xi_{l,i}\xi_{l,k} - \delta_{ik})(\xi_{n,i}\xi_{n,k} - \delta_{ik})\right. \\ & \left. + \frac{\nu}{4(1-2\nu)}(\xi_{p,l}\xi_{p,l} - 3)^2\right]. \end{aligned} \tag{5}$$

We consider the macroscopically homogeneous deformations (strain gradients $X_{i,k}$ are constant along the sample). For a given $X_{i,k}$, the strain gradients $\xi_{\mu\nu}$ take values providing the minimum of the function F. Equating the partial derivatives (with respect to $\xi_{\mu\nu}$) of this function to zero, we arrive at the system of equations determining $\xi_{\mu\nu}$:

$$\begin{aligned} & \Delta\left(\frac{1}{d^{0^2}}\xi_{\mu,k}d_k^0d_\nu^0 - \frac{1}{d^{0^2}}X_{\mu,i}R_i^0d_\nu^0\right) + \xi_{p,\nu}\xi_{p,i}\xi_{\mu,i} \\ & + \frac{\nu}{1-2\nu}\xi_{p,q}\xi_{p,q}\xi_{\mu,\nu} - \frac{\nu+1}{1-2\nu}\xi_{\mu,\nu} = 0, \\ & \Delta = \frac{3Td^0}{S^0na^2G}. \end{aligned} \tag{6}$$

Solving equations (6) allows us to calculate $\xi_{\mu\nu}$. We restrict ourselves by an approximation sufficient for applications in practice. We consider small finite macroscopic deformations and estimate the value of Δ. From the data of [2–4], the minimum value of G for cellulose and polyethylene (in the direction normal to the macromolecule orientation) is estimated as $G \sim 10^9$ N/m, $n \sim 10$, $d^0 \sim 10$ nm, $a \sim 1$ nm. Theoretical estimates [6] indicate that not more than a half of all chains existing in a polyethylene crystallite go out into the amorphous domain. Thus, not more than ten segments of macromolecules must go out from the crystallite cross section area of $25a^2$ into the amorphous domain that yields the estimate $S^0 \sim 2.5a^2$. Using these data, we find $\Delta \sim 10^{-2}$. This allows us to ignore the first term in (6) and, consequently, we have, in this approximation, $\xi_{\mu\nu} = 0$. This result corresponds to the approximation of absolutely rigid crystallites.

Thus, the model element possesses the energy

$$F = \frac{3T}{2na^2}X_{l,i}X_{l,k}R_i^0R_k^0. \tag{7}$$

Assuming that crystallites and segments of macromolecules in the amorphous domain differ only by their orientations, we write out the density of the elastic energy Φ of the sample. To do this, we average the expression (7) with respect to the equiprobable and independent orientations $\mathbf{d}^0$ and $\mathbf{l}^0$, and multiply it by the number M of segments of linking macromolecules per unit volume in the sample:

$$M = KSm, \tag{8}$$

where K is the number of crystallites per unit volume, S is the crystallite cross section perpendicular to the direction of the macromolecule orientation, m is the number of macromolecule segments extending into the amorphous domain from the crystallite unit surface.

Employing (1), (7), and (8), we obtain after simple transformations

$$\Phi = CI,$$

where I is the first invariant of the macroscopic strain tensor ($I = X_{l,i}X_{l,k}\delta_{ik}$), which was introduced similarly to [7],

$$C = \frac{KSmTl^{0^2}}{2na^2}\left[1 + \frac{\chi^2}{(1-\chi)^2}\right], \quad (9)$$

and $\chi = d^0/R^0$. Relationship (9) corresponds, in its form, to the first Mooney constant that has acquired the molecular structure interpretation for the given material.

In accordance with (9), the elastic properties for a given polymeric material are independent (in the explicit form) of the crystallite volume fraction or of the amorphous part. The degree of crystallinity is determined by the ratio of the crystallite linear size (along the orientation direction of the macromolecules) and the crystallite large period.

REFERENCES

1. V. E. Zgaevskiĭ, Dokl. Akad. Nauk **341**, 758 (1995) [Dokl. Phys. **40**, 179 (1995)].
2. B. Rosen, *Fracture Processes in Polymeric Solids* (Wiley, New York, 1969; Khimiya, Moscow, 1971).
3. R. Tjudze and T. Kawai, *Physical Chemistry of Polymers* (Khimiya, Moscow, 1977).
4. Narisava, *Strength of Polymeric Materials* (Ohmsha, Tokyo, 1982; Khimiya, Moscow, 1987).
5. L. D. Landau and E. M. Lifshitz, *Elasticity Theory* (Nauka, Moscow, 1987).
6. L. Mandelkern, *Crystallization of Polymers* (McGraw-Hill, New York, 1964; Khimiya, Moscow, 1966).
7. V. E. Zgaevskiĭ, Kolloidn. Zh. **57**, 679 (1995).

Translated by T. Galkina

Doklady Physics, Vol. 45, No. 3, 2000, pp. 108–114. Translated from Doklady Akademii Nauk, Vol. 371, No. 3, 2000, pp. 322–328.

TECHNICAL PHYSICS

Excitation of a System of Superconducting Antennas

V. F. Kravchenko*, Corresponding Member of the RAS V. I. Pustovoĭt*, N. A. Khizhnyak, and N. M. Yatsenko*****

Received June 18, 1999

The method of integral equations has a wide application in solving internal and external boundary value problems of electrodynamics [1–15]. The integral equations of electrodynamics present the boundary value problem as that with nonlocal boundary conditions. This seems to be reasonable in the case of scattering problems when the internal field (or the volume current density) is expressed directly in terms of the incident-wave field, while the scattered-wave field is found only at the second stage of construction of the solution.

Formulation of the problem and the method of solving. We consider a system of two parallel superconducting vibrators with the lengths L_1, L_2 and radii b_1, b_2. The distance between the vibrators is d, and their centers are shifted by h (Fig. 1). For definiteness, we assume both the vibrators to be placed in the *YOZ* plane and to be parallel to the *OZ*-axis. Specific features of the electromagnetic wave scattering in superconductors can be taken into account by setting the impedance boundary conditions on the surface of the vibrators. We construct a structure for the solution to the problem on the basis of integral equations of the macroscopic electrodynamics [1]. In the case of two arbitrary material bodies with the volumes V_1 and V_2, these equations have the following form:

$$\mathbf{E}(\mathbf{r}_1) = \mathbf{E}_0(\mathbf{r}_1) + \frac{1}{i\omega\varepsilon}(\mathrm{grad}\,\mathrm{div} + k_0^2\varepsilon)[\mathbf{A}_{11}(\mathbf{r}_1) + \mathbf{A}_{12}(\mathbf{r}_1)]; \quad (1)$$

$$\mathbf{E}(\mathbf{r}_2) = \mathbf{E}_0(\mathbf{r}_2) + \frac{1}{i\omega\varepsilon}(\mathrm{grad}\,\mathrm{div} + k_0^2\varepsilon)[\mathbf{A}_{22}(\mathbf{r}_2) + \mathbf{A}_{21}(\mathbf{r}_2)]; \quad (2)$$

$$\mathbf{H}(\mathbf{r}_1) = \mathbf{H}_0(\mathbf{r}_1) + \frac{k_0}{\omega}\mathrm{curl}[\mathbf{A}_{11}(\mathbf{r}_1) + \mathbf{A}_{12}(\mathbf{r}_1)]; \quad (3)$$

$$\mathbf{H}(\mathbf{r}_2) = \mathbf{H}_0(\mathbf{r}_2) + \frac{k_0}{\omega}\mathrm{curl}[\mathbf{A}_{22}(\mathbf{r}_2) + \mathbf{A}_{21}(\mathbf{r}_2)], \quad (4)$$

where

$$\mathbf{A}_{km}(\mathbf{r}_k) = \int\limits_{V_m} \frac{\mathbf{j}_m(\mathbf{r}'_m)\exp(-ik_0\sqrt{\varepsilon}|\mathbf{r}_k - \mathbf{r}'_m|)}{|\mathbf{r}_k - \mathbf{r}'_m|} d\mathbf{r}'_m; \quad (5)$$

$$k, m = 1, 2.$$

Here, $\mathbf{E}_0$ and $\mathbf{H}_0$ are strengths of the electric and magnetic fields for the given electromagnetic field; $\mathbf{E}$ and $\mathbf{H}$ are the corresponding strengths for the perturbed electromagnetic field; $k_0 = \omega/c$ is the wave number; ω is the frequency; c is the speed of light; $\mathbf{r}_k = \mathbf{r}_k(x_k, y_k, z_k)$ and $\mathbf{r}'_m = \mathbf{r}'_m(x'_m, y'_m, z'_m)$ are the radii vectors of the observation and integration points, respectively; and $\mathbf{j}_m$ is the volume density of a current induced in the mth body. Equations (1)–(4) are equivalent to the Maxwell equations and the boundary conditions on the interfaces between the media. The solution to the boundary value problem of electrodynamics involves two stages. At the

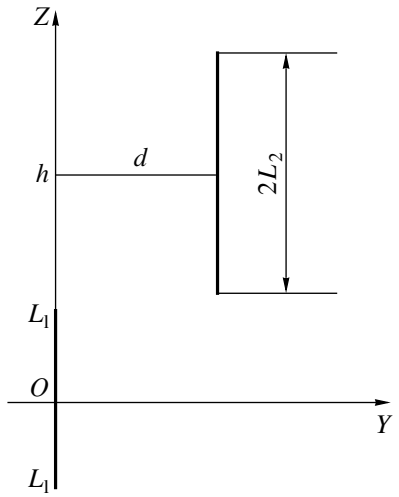

Fig. 1.

* *Institute of Radio Engineering and Electronics, Russian Academy of Sciences, ul. Mokhovaya 11, Moscow, 103907 Russia*

** *Central Design Bureau of Unique Instrumentation, Russian Academy of Sciences, ul. Butlerova 15, Moscow, 117342 Russia*

*** *Kharkov State University, pl. Dzerzhinskogo 4, Kharkov, 310077 Ukraine*

1028-3358/00/4503-0108$20.00 © 2000 MAIK “Nauka/Interperiodica”

first stage, we find the currents induced in each material body by the source field and by the field generated by the other material body. In this case, initial integral equations (1)–(4) represent the set of Fredholm inhomogeneous integral equations of the first kind with a unique solution. At the second stage, we construct the diffracted field using the already known currents. In this case, equations (1)–(4) are simply the equalities for which the total field in the left-hand side is represented as a sum of the primary field, $\mathbf{E}_0$, $\mathbf{H}_0$, and scattered fields.

Determination of currents. As we pass from arbitrary material bodies to thin linear vibrators, we take into account that only the longitudinal currents are of significance for the problem, while the transverse currents can be ignored. Projecting equations (1) and (2) onto the vibrator axes, we find the expressions for tangential components of the total electric field at the surfaces of each of the vibrators:

$$i\omega\varepsilon[E_{z1}(z_1) - E_{0z1}(z_1)] = \left(\frac{\partial^2}{\partial z_1^2} + k^2\right) \times \left\{\int_{V_1} \frac{j_{1z}(\mathbf{r}_1')\exp(-ik|\mathbf{r}_1 - \mathbf{r}_1'|)}{|\mathbf{r}_1 - \mathbf{r}_1'|} d\mathbf{r}_1' + \int_{V_2} \frac{j_{2z}(\mathbf{r}_2')\exp(-ik|\mathbf{r}_1 - \mathbf{r}_2'|)}{|\mathbf{r}_1 - \mathbf{r}_2'|} d\mathbf{r}_2'\right\}; \quad (6)$$

$$i\omega\varepsilon[E_{z2}(z_2) - E_{0z2}(z_2)] = \left(\frac{\partial^2}{\partial z_2^2} + k^2\right) \times \left\{\int_{V_2} \frac{j_{2z}(\mathbf{r}_2')\exp(-ik|\mathbf{r}_2 - \mathbf{r}_2'|)}{|\mathbf{r}_2 - \mathbf{r}_2'|} d\mathbf{r}_2' + \int_{V_1} \frac{j_{1z}(\mathbf{r}_1')\exp(-ik|\mathbf{r}_2 - \mathbf{r}_1'|)}{|\mathbf{r}_2 - \mathbf{r}_1'|} d\mathbf{r}_1'\right\}, \quad (7)$$

where $k = k_0\sqrt{\varepsilon}$.

As far as the first integral terms in (6) and (7) have singularities in the case of coincident observation and integration points, we isolate them considering the electrostatic parts of the corresponding integrals. As a result, after a sequence of manipulations, we obtain the equations for currents in each antenna, which contain small parameters. With allowance for the impedance boundary conditions $E_{z1}(z_1) = Z_1 I_1(z_1)$ and $E_{z2}(z_2) = Z_2 I_2(z_2)$ valid at the surfaces of the superconductors (Z_k is the corresponding component of the surface-impedance tensor $\hat{Z}_k$ for the kth vibrator, $k = 1, 2$), these equations take the following form:

$$\frac{d^2 I_1(z_1)}{dz_1^2} + k^2 I_1(z_1) = \alpha_1\{i\omega\varepsilon[E_{0z1}(z_1) - Z_1 I_1(z_1)] + F_{11}(z_1, I_1) + F_{12}(z_1, I_2)\}; \quad (8)$$

$$\frac{d^2 I_2(z_2)}{dz_2^2} + k^2 I_2(z_2) = \alpha_2\{i\omega\varepsilon[E_{0z2}(z_2) - Z_2 I_2(z_2)] + F_{22}(z_2, I_2) + F_{21}(x_2, I_1)\}, \quad (9)$$

where $\alpha_k = -\dfrac{1}{2\ln(2L_k/b_k)}$ are small parameters;

$$F_{11}(z_1, I_1) = \left(\frac{d^2}{dz_1^2} + k^2\right) \times \int_{-L_1}^{L_1} \frac{I_1(z_1')\exp\left(-ik\sqrt{(z_1 - z_1')^2 + b_1^2}\right) - I_1(z_1)}{\sqrt{(z_1 - z_1')^2 + b_1^2}} dz_1';$$

$$F_{22}(z_2, I_2) = \left(\frac{d^2}{dz_2^2} + k^2\right) \times \int_{-L_2 + h}^{L_2 + h} \frac{I_2(z_2')\exp\left(-ik\sqrt{(z_2 - z_2')^2 + b_2^2}\right) - I_2(z_2)}{\sqrt{(z_2 - z_2')^2 + b_2^2}} dz_2';$$

$$F_{12}(z_1, I_2) = -\frac{dI_2(z_2')}{dz_2'} \times \frac{\exp\left(-ik\sqrt{(z_1 - z_2')^2 + d^2}\right)}{\sqrt{(z_1 - z_2')^2 + d^2}}\Bigg|_{z_2' = -L_2 + h}^{z_2' = L_2 + h} + \int_{-L_2 + h}^{L_2 + h}\left[\frac{d^2 I_2(z_2')}{dz_2'^2} + k^2 I_2(z_2')\right] \times \frac{\exp\left(-ik\sqrt{(z_1 - z_2')^2 + d^2}\right)}{\sqrt{(z_1 - z_2')^2 + d^2}} dz_2';$$

$$F_{21}(z_2, I_1) = -\frac{dI_1(z_1')}{dz_1'} \times \frac{\exp\left(-ik\sqrt{(z_2 - z_1')^2 + d^2}\right)}{\sqrt{(z_2 - z_1')^2 + d^2}}\Bigg|_{z_1' = -L_1}^{z_1' = L_1}$$

$$+\int_{-L_1}^{L_1}\left[\frac{d^2I_1(z_1')}{dz_1'^2}+k^2I_1(z_1')\right]$$

$$\times\frac{\exp\left(-ik\sqrt{(z_2-z_1')^2+d^2}\right)}{\sqrt{(z_2-z_1')^2+d^2}}dz_1'.$$

According to (8), the current at an arbitrary point z_1 of the first antenna is determined by the given source field $E_{0z1}(z_1)$; its proper field $F_{11}(z_1, I_1)$ generated by the currents in other sections of the first antenna, and by the field $F_{12}(z_1, I_2)$ generated by the currents in the second antenna. The functions $E_{0z2}(z_2)$, $F_{22}(z_2, I_2)$, and $F_{21}(z_2, I_1)$ entering into equation (9) have a similar meaning. An approximate solution to each of equations (8) and (9) can be constructed by the perturbative method [2] as a power series of α_k, $k = 1, 2$. However, using this method, we arrive at different formulas for currents in the case of resonant and nonresonant vibrators. Moreover, the resonance formula turns out to be approximate in a number of cases and makes it impossible to determine the amplitude of the current. In spite of the proper and mutual fields of antennas, which enter into the right-hand side of equations (8) and (9), the nonresonant formula is independent of them. The solution suitable for resonant and nonresonant antennas was obtained in [3, 4] by the partial-averaging methods in investigating isolated linear vibrators. In this paper, the partial-averaging method [3] is applied for solving equations describing currents in a system of two parallel superconducting vibrators. Solving equations (8) and (9) by the method of variation of arbitrary constants, we obtain the following results:

$$I_1(z_1) = A_1(z_1)\cos kz_1 + B_1(z_1)\sin kz_1; \quad (10)$$

$$I_2(z_2) = A_2(z_2)\cos kz_2 + B_2(z_2)\sin kz_2; \quad (11)$$

$$\frac{dI_1(z_1)}{dz_1} = -A_1(z_1)k\sin kz_1 + B_1(z_1)k\cos kz_1; \quad (12)$$

$$\frac{dI_2(z_2)}{dz_2} = -A_2(z_2)k\sin kz_2 + B_2(z_2)k\cos kz_2. \quad (13)$$

The coefficients $A_1(z_1)$, $B_1(z_1)$, $A_2(z_2)$, and $B_2(z_2)$ are found from the equations

$$\frac{dA_1(z_1)}{dz_1} = -\alpha_1 f_1(z_1)\sin kz_1 + \frac{\alpha_1 i\omega\sqrt{\varepsilon}Z_1}{k_0}[A_1(z_1)\cos kz_1 + B_1(z_1)\sin kz_1]\sin kz_1; \quad (14)$$

$$\frac{dB_1(z_1)}{dz_1} = \alpha_1 f_1(z_1)\cos kz_1 - \frac{\alpha_1 i\omega\sqrt{\varepsilon}Z_1}{k_0} \times [A_1(z_1)\cos kz_1 + B_1(z_1)\sin kz_1]\cos kz_1; \quad (15)$$

$$\frac{dA_2(z_2)}{dz_2} = -\alpha_2 f_2(z_2)\sin kz_2 + \frac{\alpha_2 i\omega\sqrt{\varepsilon}Z_2}{k_0} \times [A_2(z_2)\cos kz_2 + B_2(z_2)\sin kz_2]\sin kz_2; \quad (16)$$

$$\frac{dB_2(z_2)}{dz_2} = \alpha_2 f_2(z_2)\cos kz_2 - \frac{\alpha_2 i\omega\sqrt{\varepsilon}Z_2}{k_0} \times [A_2(z_2)\cos kz_2 + B_2(z_2)\sin kz_2]\cos kz_2, \quad (17)$$

where

$$f_1(z_1) = \frac{i\omega\sqrt{\varepsilon}}{k_0}E_{0z1}(z_1) + \frac{F_{11}[z_1, A_1, B_1]}{\sqrt{\varepsilon}} + \frac{F_{12}[z_1, A_2, B_2]}{\sqrt{\varepsilon}}$$

and

$$f_2(z_2) = \frac{i\omega\sqrt{\varepsilon}}{k_0}E_{0z2}(z_2) + \frac{F_{22}[z_2, A_2, B_2]}{\sqrt{\varepsilon}} + \frac{F_{21}[z_2, A_1, B_1]}{\sqrt{\varepsilon}}.$$

The set of equations (14)–(17) is completely equivalent to (8) and (9). It belongs to the set of integro-differential equations written out in the standard form and is not solved with respect to derivatives. Using the well-known schemes [3, 8], we average this set over the z_1 and z_2 variables explicitly entering into it. This averaging is quite justified because all the functions standing in the right-hand sides of equations (14)–(17) are bounded in their definition domain. They are continuous with respect to the z_1 and z_2 variables, and satisfy the Lipschitz conditions with respect to A_1, B_1, A_2, and B_2. As a result of averaging, we obtain the following set of inhomogeneous differential equations:

$$\begin{aligned}
\frac{d\bar{A}_1(z_1)}{dz_1} &= -\alpha_1\sqrt{\varepsilon}\,\overline{f}_1(z_1)\sin kz_1 + \kappa_1\bar{B}_1(z_1),\\
\frac{d\bar{B}_1(z_1)}{dz_1} &= \alpha_1\sqrt{\varepsilon}\,\overline{f}_1(z_1)\cos kz_1 - \kappa_1\bar{A}_1(z_1),\\
\frac{d\bar{A}_2(z_2)}{dz_2} &= -\alpha_2\sqrt{\varepsilon}\,\overline{f}_2(z_2)\sin kz_2 + \kappa_2\bar{B}_2(z_2),\\
\frac{d\bar{B}_2(z_2)}{dz_2} &= \alpha_2\sqrt{\varepsilon}\,\overline{f}_2(z_2)\cos kz_2 - \kappa_2\bar{A}_2(z_2),
\end{aligned} \quad (18)$$

where the bar sign over the corresponding function denotes its averaged value;

$$\kappa_1 = \alpha_1\frac{i\omega\sqrt{\varepsilon}}{2k_0}Z_1, \quad \kappa_2 = \alpha_2\frac{i\omega\sqrt{\varepsilon}}{2k_0}Z_2,$$

$$Z_1 = R_1 + iX_1, \quad Z_2 = R_2 + iX_2,$$

$$\bar{f}_2(z_2) = \frac{i\omega\sqrt{\varepsilon}}{k_0}E_{0z2}(z_2) + \bar{F}_{22}(z_2, \bar{A}_2, \bar{B}_2) + \bar{F}_{21}(z_2, \bar{A}_1, \bar{B}_1),$$

$$\bar{f}_1(z_1) = \frac{i\omega\sqrt{\varepsilon}}{k_0}E_{0z1}(z_1) + \bar{F}_{11}(z_1, \bar{A}_1, \bar{B}_1) + \bar{F}_{12}(z_1, \bar{A}_2, \bar{B}_2).$$

Here,

$$\bar{F}_{11}(z_1, \bar{A}_1, \bar{B}_1) = [\bar{A}_1(L_1)\sin kL_1 - \bar{B}_1(L_1)\cos kL_1] \times \frac{\exp\left(-ik\sqrt{(z_1 - L_1)^2 + b_1^2}\right)}{\sqrt{(z_1 - L_1)^2 + b_1^2}} + [\bar{A}_1(-L_1)\sin kL_1 + \bar{B}_1(-L_1)\cos kL_1] \times \frac{\exp\left(-ik\sqrt{(z_1 + L_1)^2 + b_1^2}\right)}{\sqrt{(z_1 + L_1)^2 + b_1^2}};$$

$$\bar{F}_{12}(z_1, \bar{A}_2, \bar{B}_2) = [\bar{A}_2(L_2 + h)\sin k(L_2 + h) - \bar{B}_2(L_2 + h)\cos k(L_2 + h)] \times \frac{\exp\left(-ik\sqrt{(z_1 - L_2 - h)^2 + d^2}\right)}{\sqrt{(z_1 - L_2 - h)^2 + d^2}} - [\bar{A}_2(-L_2 + h)\sin k(-L_2 + h) - \bar{B}_2(-L_2 + h)\cos k(-L_2 + h)] \times \frac{\exp\left(-ik\sqrt{(z_1 + L_2 - h)^2 + d^2}\right)}{\sqrt{(z_1 + L_2 - h)^2 + d^2}};$$

$$\bar{F}_{22}(z_2, \bar{A}_2, \bar{B}_2) = [\bar{A}_2(L_2 + h)\sin k(L_2 + h) - \bar{B}_2(L_2 + h)\cos k(L_2 + h)] \times \frac{\exp\left(-ik\sqrt{(z_2 - L_2 - h)^2 + b_2^2}\right)}{\sqrt{(z_2 - L_2 - h)^2 + b_2^2}} - [\bar{A}_2(-L_2 + h)\sin k(-L_2 + h) - \bar{B}_2(-L_2 + h)\cos k(-L_2 + h)] \times \frac{\exp\left(-ik\sqrt{(z_2 + L_2 - h)^2 + b_2^2}\right)}{\sqrt{(z_2 + L_2 - h)^2 + b_2^2}};$$

$$\bar{F}_{21}(z_2, \bar{A}_1, \bar{B}_1) = [\bar{A}_1(L_1)\sin kL_1 - \bar{B}_1(L_1)\cos kL_1] \times \frac{\exp\left(-ik\sqrt{(z_2 - L_1)^2 + d^2}\right)}{\sqrt{(z_2 - L_1)^2 + d^2}} + [\bar{A}_1(-L_1)\sin kL_1 + \bar{B}_1(-L_1)\cos kL_1] \times \frac{\exp\left(-ik\sqrt{(z_2 + L_1)^2 + d^2}\right)}{\sqrt{(z_2 + L_1)^2 + d^2}}.$$

Integrating equations (18)–(21) and substituting the averaged values $\bar{A}_1(z_1)$, $\bar{B}_1(z_1)$, $\bar{A}_2(z_2)$, and $\bar{B}_2(z_2)$ instead of $A_1(z_1)$, $B_1(z_1)$, $A_2(z_2)$, and $B_2(z_2)$ into (10) and (11) found above, we obtain asymptotic expressions for currents in the system of two thin parallel superconducting antennas in the case of an arbitrary excitation:

$$\begin{aligned} I_1(z_1) &= \bar{A}_1(-L_1)\cos[\tilde{k}_1(z_1 + L_1) - kL_1] + \bar{B}_1(-L_1)\sin[\tilde{k}_1(z_1 + L_1) - kL_1] \\ &+ \alpha_1\sqrt{\varepsilon}\int_{-L_1}^{z_1}\bar{f}_1(z_1')\sin\tilde{k}_1(z_1 - z_1')dz_1', \\ I_2(z_2) &= \bar{A}_2(-L_2 + h)\cos[\tilde{k}_2(z_2 + L_2) - kL_2 - \kappa_2 h] \\ &+ \bar{B}_2(-L_2 + h)\sin[\tilde{k}_2(z_2 + L_2) - kL_2 - \kappa_2 h] \\ &+ \alpha_2\sqrt{\varepsilon}\int_{-L_2 + h}^{z_2}\bar{f}_2(z_2')\sin\tilde{k}_2(z_2 - z_2')dz_2'. \end{aligned} \quad (19)$$

In these formulas, $\tilde{k}_1$ and $\tilde{k}_2$ are the complex wave numbers:

$$\tilde{k}_1 = k + \kappa_1 = \tilde{k}_1' + i\tilde{k}_1'', \quad \tilde{k}_2 = k + \kappa_2 = \tilde{k}_2' + i\tilde{k}_2'',$$

where

$$\tilde{k}_1' = k_0\sqrt{\varepsilon}\left(1 - \alpha_1\frac{\bar{X}_1}{k_0 b_1}\right),$$

$$\tilde{k}_1'' = k_0\sqrt{\varepsilon}\left(\alpha_1\frac{\bar{R}_1}{k_0 b_1}\right), \quad \tilde{k}_2' = k_0\sqrt{\varepsilon}\left(1 - \alpha_2\frac{\bar{X}_2}{k_0 b_2}\right),$$

$$\tilde{k}_2'' = k_0\sqrt{\varepsilon}\left(\alpha_2\frac{\bar{R}_2}{k_0 b_2}\right),$$

$$\bar{Z}_1 = \bar{R}_1 + i\bar{X}_1 = \frac{R_1 + iX_1}{4\pi k_0/\omega},$$

and

$$\bar{Z}_2 = \bar{R}_2 + i\bar{X}_2 = \frac{R_2 + iX_2}{4\pi k_0/\omega}$$

are the values of surface impedances normalized to the wave resistance of the free space. The presence of real

parts of the surface impedances implies attenuating the current amplitudes in the antennas. A change in the imaginary parts of the surface impedances of the superconducting vibrators affects the resonance frequency. The coefficients $\bar{A}_1(-L_1)$, $\bar{B}_1(-L_1)$, $\bar{A}_2(-L_2 + h)$, and $\bar{B}_2(-L_2 + h)$ are found from the conditions of current vanishing at the vibrator ends, and the symmetry conditions associated with the method of exciting the vibrators.

Relationships for currents. In the case of exciting the vibrators by the plane electromagnetic-wave field $\{E_{0z1}(z_1) = E_{0z2}(z_2) = E_0\}$, the expressions for currents have the form

$$
\begin{aligned}
I_1(z_1) &= -\alpha_1 \frac{2E_0}{\tilde{k}_1} \frac{i\omega\sqrt{\varepsilon}/k_0}{\tilde{D}_{11}\tilde{D}_{22} - \alpha_1\alpha_2\tilde{M}_{12}\tilde{M}_{21}} \\
&\times \{\tilde{D}_{22}\sin\tilde{k}_1L_1(\cos\tilde{k}_1z_1 - \cos\tilde{k}_1L_1) \\
&+ \alpha_2(\tilde{k}_1/\tilde{k}_2)\sin^2\tilde{k}_2L_2 \\
&\times [\tilde{U}_{12}(z_1)\sin 2\tilde{k}_1L_1 - \tilde{M}_{12}\sin\tilde{k}_1(L_1 + z_1)]\}, \\
I_2(z_2) &= -\alpha_2 \frac{2E_0}{\tilde{k}_2} \frac{i\omega\sqrt{\varepsilon}/k_0}{\tilde{D}_{11}\tilde{D}_{22} - \alpha_1\alpha_2\tilde{M}_{12}\tilde{M}_{21}} \\
&\times \{\tilde{D}_{11}\sin\tilde{k}_2L_2(\cos\tilde{k}_2(z_2 - h) - \cos\tilde{k}_2L_2) \\
&+ \alpha_1(\tilde{k}_2/\tilde{k}_1)\sin^2\tilde{k}_1L_1 \\
&\times [\tilde{U}_{21}(z_2)\sin 2\tilde{k}_2L_2 - \tilde{M}_{21}\sin\tilde{k}_2(L_2 + z_2 - h)]\},
\end{aligned}
\tag{20}
$$

where

$$
\begin{aligned}
\tilde{U}_{12}(z_1) &= \int_{k(L_2 + h - z_1)}^{k(L_2 + h + L_1)} \frac{\exp\left(-i\sqrt{x^2 + k^2d^2}\right)}{\sqrt{x^2 + k^2d^2}} \\
&\times \sin\tilde{k}_1\left(z_1 - L_2 - h + \frac{x}{k}\right)dx \\
&+ \int_{k(L_2 - h - L_1)}^{k(L_2 - h + z_1)} \frac{\exp\left(-i\sqrt{x^2 + k^2d^2}\right)}{\sqrt{x^2 + k^2d^2}} \\
&\times \sin\tilde{k}_1\left(z_1 + L_2 - h - \frac{x}{k}\right)dx, \\
\tilde{U}_{21}(z_2) &= \int_{k(L_1 - z_2)}^{k(L_1 + L_2 - h)} \frac{\exp\left(-i\sqrt{x^2 + k^2d^2}\right)}{\sqrt{x^2 + k^2d^2}} \\
&\times \sin\tilde{k}_2\left(z_2 - L_2 + \frac{x}{k}\right)dx \\
&+ \int_{k(L_1 - L_2 + h)}^{k(L_1 + z_2)} \frac{\exp\left(-i\sqrt{x^2 + k^2d^2}\right)}{\sqrt{x^2 + k^2d^2}} \\
&\sin\tilde{k}_2\left(z_2 + L_1 - \frac{x}{k}\right)dx,
\end{aligned}
$$

$$
\begin{aligned}
\tilde{D}_{11} &= \sin 2\tilde{k}_1L_1 + \alpha_1\tilde{M}_{11}; \\
\tilde{D}_{22} &= \sin 2\tilde{k}_2L_2 + \alpha_2\tilde{M}_{22}; \\
\tilde{M}_{11} &= 2\sin\tilde{k}_1L_1 \\
&\times \int_0^{2kL_1} \frac{\exp\left(-i\sqrt{x^2 + k^2b_1^2}\right)}{\sqrt{x^2 + k^2b_1^2}} \cos\tilde{k}_1\left(L_1 - \frac{x}{k}\right)dx; \\
\tilde{M}_{22} &= 2\sin\tilde{k}_2L_2 \int_0^{2kL_2} \frac{\exp\left(-i\sqrt{x^2 + k^2b_2^2}\right)}{\sqrt{x^2 + k^2b_2^2}} \\
&\times \cos\tilde{k}_2\left(L_2 - \frac{x}{k}\right)dx;
\end{aligned}
$$

$$
\tilde{M}_{12} = \tilde{U}_{12}(z_1 = L_1); \quad \tilde{M}_{21} = \tilde{U}_{21}(z_2 = L_2 + h).
$$

The formulas for the currents are valid in the most general case, when the lengths of vibrators and the distances between them are arbitrary. The mutual effect of the vibrators on the currents is described by the functions $\tilde{U}_{12}$ and $\tilde{U}_{21}$. As one of the vibrators is removed to infinity ($d \longrightarrow \infty$), we obtain the well-known formulas [15] for the current in an isolated vibrator. For two active vibrators excited under conditions of cophasing, i.e., $\{E_{0z1}(z_1) = V_{01}\delta(z_1)$ and $E_{0z2}(z_2) = V_{02}\delta(z_2 - h)\}$, the expressions for currents have the following form:

$$
\begin{aligned}
I_1(z_1) &= -\alpha_1 V_{01} \frac{i\omega\sqrt{\varepsilon}/k_0}{\tilde{D}_{11}\tilde{D}_{22} - \alpha_1\alpha_2\tilde{M}_{12}\tilde{M}_{21}} \\
&\times \{\tilde{D}_{22}\sin\tilde{k}_1L_1\sin\tilde{k}_1(L_1 - |z_1|) \\
&+ \alpha_2\frac{2E_{02}}{\tilde{k}_2V_{01}}\sin^2\tilde{k}_2L_2 \\
&\times [\tilde{U}_{12}(z_1)\sin 2\tilde{k}_1L_1 - \tilde{M}_{12}\sin\tilde{k}_1(L_1 + z_1)]\}, \\
I_2(z_2) &= -\alpha_2\frac{E_{02}}{\tilde{k}_2} \frac{i\omega\sqrt{\varepsilon}/k_0}{\tilde{D}_{11}\tilde{D}_{22} - \alpha_1\alpha_2\tilde{M}_{12}\tilde{M}_{21}} \\
&\times \{\tilde{D}_{11} \times 2\sin\tilde{k}_2L_2[\cos\tilde{k}_2(z_2 - h) - \cos\tilde{k}_2L_2]
\end{aligned}
$$

$$+\alpha_1\frac{V_{01}\tilde{k}_2}{E_{02}}\sin\tilde{k}_1L_1$$
$$\times[\tilde{U}_{21}(z_2)\sin2\tilde{k}_2L_2-\tilde{M}_{21}\sin\tilde{k}_2(L_2+z_2-h)]\}.$$

We should bear in mind that, in order to find the current at the center of the first and second vibrators, it is necessary to substitute $z_1 = 0$ and $z_2 = h$ into expressions (20). The choice $z_2 = h$ is explained by the fact that the center of the second vibrator is shifted by the distance h with respect to the center of the first one.

Radiation fields. The radiation fields at an arbitrary point **r**, which belongs to none of the vibrators, can be found by substituting the expressions obtained for the currents into equations (1) and (3) [or (2) and (4). When the radiation fields are considered in the far-field zone of the antenna system under investigation, expressions (5) take the following form:

$$\mathbf{A}_{11}(\mathbf{r}) = \mathbf{e}_z\frac{\exp(-ikr)}{r}\Pi_{11}(\theta);$$
$$\mathbf{A}_{12}(\mathbf{r}) = \mathbf{e}_z\frac{\exp(-ikr)}{r}\Pi_{12}(\theta) \quad (21)$$
$$\times\exp[-ik(h\cos\theta+d\sin\theta\cos\varphi)],$$

where

$$\Pi_{11}(\theta) = \int_{-L_1}^{L_1} I_1(z_1)\exp(-ikz_1\cos\theta)dz_1,$$
$$\Pi_{12}(\theta) = \int_{-L_2+h}^{L_2+h} I_2(z_2)\exp(-ikz_2\cos\theta)dz_2. \quad (22)$$

Substituting (21) and (22) into expressions (1) and (3) for the fields, and restricting ourselves by only terms on the order of $1/r$, we find the fields in the far-field zone:

$$E_r = E_\varphi = H_r = H_\theta = 0,$$
$$E_\theta = -\frac{k^2}{i\omega\varepsilon}\sin\theta\frac{\exp(-ikr)}{r}\Pi(\theta,\varphi), \quad (23)$$
$$H_\varphi = -\frac{k^2}{i\omega\sqrt{\varepsilon}}\sin\theta\frac{\exp(-ikr)}{r}\Pi(\theta,\varphi),$$

where

$$\Pi(\theta,\varphi)$$
$$=\Pi_{11}(\theta)+\Pi_{12}(\theta)\exp[-ik(h\cos\theta+d\sin\theta\cos\varphi)].$$

With allowance for expressions (23) obtained for the radiation fields, the power-flux density has the form

$$S = \frac{ck_0^4\sqrt{\varepsilon}}{8\pi r^2\omega^2}|\Pi(\theta,\varphi)|^2\sin^2\theta.$$

Numerical experiment. We calculated the current distribution along one of the vibrators in the system of

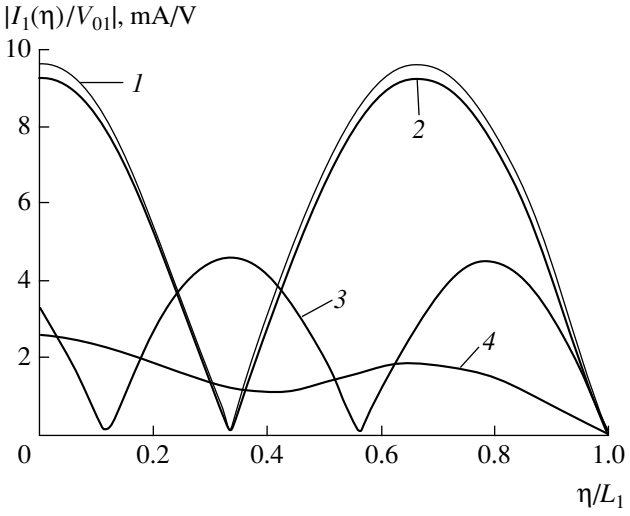

Fig. 2.

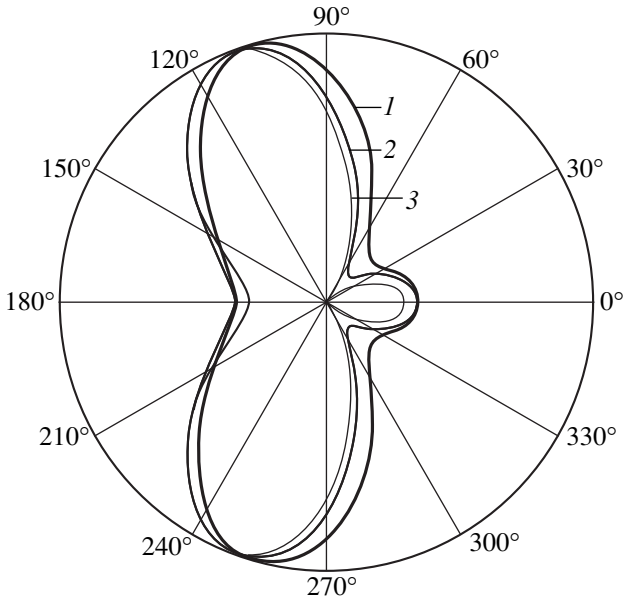

Fig. 3.

sesquialteral wavelength vibrators ($L/\lambda = 0.75$), arranged at a distance $d = \lambda$, as a function of the complex surface impedance (normalized to 120π) for $Z_1 = Z_2$. Curves in Fig. 2 correspond to the following cases: (*1*) perfectly conducting vibrators, (*2*) superconductors made of niobium $(0.1676 \times 10^{-4} + i \times 0.303 \times 10^{-2})/120\pi$ [9], (*3*) vibrators with the purely imaginary surface impedance $Z = 0 + i \times 0.3$, and (*4*) vibrators with the real impedance $Z = 0.1 + i \times 0$. The appearance of the complex surface impedance leads to a change in both the amplitude and type of the current distribution function. It is of special importance to emphasize that a change in the imaginary part of the surface impedance results in a variation in the resonance frequency of the antenna

(a change in the position of zeros in the current distribution along the vibrator), which can be used for detecting the superconductivity. The increase in the real part of the surface impedance results in both decreasing the amplitude and distorting the shape of the current due to the Joule loss. We have considered also a system of passive vibrators of various lengths ($L_1 = 0.25\lambda$ and $L_2 = 0.5\lambda$) placed at a distance $d = 0.5\lambda$ and $h = 0$. Using formulas (20) and (23), we plotted the power directivity patterns in the plane perpendicular to the vibrators (Fig. 3) as a function of the normalized complex surface impedances for $Z_1 = Z_2$. The curves in Fig. 3 correspond to the following cases: (*1*) superconducting vibrators made of niobium; (*2*) and (*3*) impedance vibrators with impedances of $0.05 + i \times 0.3$ and $0.1 + i \times 0$, respectively. Increasing the active part of the surface impedance of the antennas results in the disappearance of the zeros in the directivity pattern.

Thus, we have shown the efficiency of the method of integral equations, which makes it possible to analytically solve, in the general form, the problem of excitation of a current, and also the determination of the radiation fields for two parallel superconducting antennas. An extension of the method presented here to the investigation of antenna arrays with a larger number of vibrators causes no principal difficulties.

REFERENCES

1. N. A. Khizhnyak, *Integral Equations of Macroscopic Electrodynamics* (Naukova Dumka, Kiev, 1986).
2. M. A. Leontovich and M. L. Levin, Zh. Tekh. Fiz. **14**, 481 (1944).
3. Yu. A. Mitropol'skiĭ, Ukr. Mat. Zh., No. 1, 30 (1972).
4. V. F. Kravchenko, in *Proceedings of the International Conference on Operator Theory and Its Application to Scientific and Industrial Problems*, Winnipeg, Canada, 1998 (Winnipeg, Canada, 1998), p. 49.
5. V. F. Kravchenko, in *Proceedings of the IMA Conference on Boundary Integral Methods: Theory and Applications*, Salford, UK, 1997 (Salford, UK, 1997), p. 4.
6. Yu. V. Gandel', V. F. Kravchenko, and N. V. Morozova, Electromag. Waves and Electron. Syst. **2**, 4 (1997).
7. Yu. V. Gandel', V. F. Kravchenko, and V. I. Pustovoĭt, Dokl. Math. **54**, 959 (1996).
8. V. F. Kravchenko, Dokl. Akad. Nauk SSSR **309**, 594 (1989) [Sov. Phys.–Dokl. **34**, 983 (1989)].
9. V. F. Kravchenko, Dokl. Akad. Nauk **328**, 272 (1993) [Dokl. Phys. **38**, 22 (1993)].
10. V. F. Kravchenko and V. T. Erofeenko, Dokl. Math. **53**, 429 (1996).
11. V. F. Kravchenko and R. G. Tyutyukin, Radiotekhnika, No. 2, 8 (1997).
12. V. F. Kravchenko and A. B. Kazarov, Zarubezhn. Radioélektronika. Usp. Sovrem. Radioélectroniki, No. 11, 59 (1997).
13. V. F. Kravchenko and G. L. Sidel'nikov, Dokl. Akad. Nauk **361**, 185 (1998) [Dokl. Phys. **43**, 408 (1998)].
14. I. K. Lifanov, *Method of Singular Integral Equations and Numerical Experiment* (Yanus, Moscow, 1995).
15. N. N. Gorobets, V. A. Petlenko, and N. A. Khizhnyak, in *Scientific and Methodological Papers on Applied Electrodynamics* (Izd. MEI, Moscow, 1983), No. 6.

Translated by V. Bukhanov

Doklady Physics, Vol. 45, No. 3, 2000, pp. 115–117. Translated from Doklady Akademii Nauk, Vol. 371, No. 1, 2000, pp. 49–51.

MECHANICS

Isotropy Conditions and the Generalized Associate Law of Plastic Flow

D. D. Ivlev*, Academician A. Yu. Ishlinskiĭ, and L. A. Maksimova***

Received October 8, 1999

1. The isotropy conditions of continuum, for which stress (σ_{ij}) and strain-rate (ε_{ij}) tensors are defined in an orthogonal system of coordinates, have the form [1]

$$\begin{aligned}\sigma_x\varepsilon_{xy} + \tau_{xy}\varepsilon_y + \tau_{xz}\varepsilon_{yz} &= \tau_{xy}\varepsilon_x + \sigma_y\varepsilon_{xy} + \tau_{yz}\varepsilon_{xz},\\ \tau_{xy}\varepsilon_{xz} + \sigma_y\varepsilon_{yz} + \tau_{yz}\varepsilon_z &= \tau_{xz}\varepsilon_{xy} + \tau_{yz}\varepsilon_y + \sigma_z\varepsilon_{yz},\\ \tau_{xz}\varepsilon_x + \tau_{yz}\varepsilon_{xy} + \sigma_z\varepsilon_{xz} &= \sigma_x\varepsilon_{xz} + \tau_{xy}\varepsilon_{yz} + \tau_{xz}\varepsilon_z.\end{aligned} \quad (1.1)$$

Furthermore, we consider an isotropic perfectly plastic medium obeying the equilibrium equations

$$\begin{aligned}\frac{\partial\sigma_x}{\partial x} + \frac{\partial\tau_{xy}}{\partial y} + \frac{\partial\tau_{xz}}{\partial z} &= 0,\\ \frac{\partial\tau_{xy}}{\partial x} + \frac{\partial\sigma_y}{\partial y} + \frac{\partial\tau_{yz}}{\partial z} &= 0,\\ \frac{\partial\tau_{xz}}{\partial x} + \frac{\partial\tau_{yz}}{\partial y} + \frac{\partial\sigma_z}{\partial z} &= 0,\end{aligned} \quad (1.2)$$

the plasticity conditions

$$f_k(\sigma_{ij}) = 0, \quad (1.3)$$

and the associate law of plastic flow

$$\varepsilon_{ij} = \lambda_k\frac{\partial f_k}{\partial\sigma_{ij}}, \quad \lambda_k \geq 0, \quad (1.4)$$

where the summation is carried out over the subscript k.

Using the Eulerian representation for the medium flow, we write out the relation between the components of the tensor ε_{ij} and the translational-velocity components u, v, and w:

$$\varepsilon_x = \frac{\partial u}{\partial x}, \quad \varepsilon_y = \frac{\partial v}{\partial y}, \quad \varepsilon_z = \frac{\partial w}{\partial z},$$

$$\varepsilon_{xy} = \frac{1}{2}\left(\frac{\partial u}{\partial y} + \frac{\partial v}{\partial x}\right), \quad \varepsilon_{xz} = \frac{1}{2}\left(\frac{\partial u}{\partial z} + \frac{\partial w}{\partial x}\right), \quad (1.5)$$

$$\varepsilon_{yz} = \frac{1}{2}\left(\frac{\partial v}{\partial z} + \frac{\partial w}{\partial y}\right).$$

We assume that the plastic state is determined by a single smooth yield function

$$f(\sigma_{ij}) = 0. \quad (1.6)$$

According to (1.4) and (1.6),

$$\varepsilon_{ij} = \lambda\frac{\partial f}{\partial\sigma_{ij}}, \quad \lambda \geq 0. \quad (1.7)$$

We restrict ourselves to the case of an incompressible material. Then,

$$\varepsilon_x + \varepsilon_y + \varepsilon_z = 0, \quad \frac{\partial f}{\partial\sigma_x} + \frac{\partial f}{\partial\sigma_y} + \frac{\partial f}{\partial\sigma_z} = 0. \quad (1.8)$$

We now have eight equations (1.1), (1.2), (1.6), and (1.8) to determine nine unknowns presented by six stress components σ_{ij} and three velocity components u, v, and w. The missing expression, for example,

$$\frac{\varepsilon_x}{\partial f/\partial\sigma_x} = \frac{\varepsilon_y}{\partial f/\partial\sigma_y} \quad (1.9)$$

can be derived from two arbitrary relations in (1.7) by means of elimination of the quantity λ. Consequently, for a smooth yield surface in the case of an isotropic perfectly plastic body, application of the isotropy conditions (1.1) may be accompanied by using, in part, relations of the flow associate law (1.9).

We consider a plasticity condition in the form

$$\begin{aligned}a\sigma_1 + b\sigma_2 + c\sigma_3 &= \kappa,\\ a + b + c = 0, \quad a, b, c, \kappa &= \text{const}.\end{aligned} \quad (1.10)$$

Then, it follows from equations (1.7) and (1.10):

$$\begin{aligned}\varepsilon_1 = \lambda a, \quad \varepsilon_2 &= \lambda b,\\ \varepsilon_3 = \lambda c, \quad \varepsilon_1 + \varepsilon_2 + \varepsilon_3 &= 0.\end{aligned} \quad (1.11)$$

Expressions (1.11) lead to the following representations of the second (I_2) and third (I_3) invariants of the

* *Chuvash State Pedagogical University, ul. Karla Marksa 38, Cheboksary, 428000 Russia*

** *Institute for Problems in Mechanics, Russian Academy of Sciences, pr. Vernadskogo 101, Moscow, 117526 Russia*

1028-3358/00/4503-0115$20.00

strain-rate tensor:

$$I_2 = \varepsilon_{ij}\varepsilon_{ij} = \varepsilon_1\varepsilon_2 + \varepsilon_2\varepsilon_3 + \varepsilon_3\varepsilon_1 = \lambda^2(ab + bc + ca), \quad (1.12)$$

$$I_3 = \varepsilon_{ij}\varepsilon_{jk}\varepsilon_{ki} = \lambda^3 abc. \quad (1.13)$$

In turn, expressions (1.12) and (1.13) yield the equation

$$\left(\frac{I_3}{abc}\right)^2 - \left(\frac{I_3}{ab + bc + ca}\right)^3 = 0, \quad (1.14)$$

which can be used instead of (1.9).

For the Tresca plasticity condition

$$\sigma_1 - \sigma_2 = 2\kappa, \quad \sigma_2 \le \sigma_3 \le \sigma_1 \quad (1.15)$$

in accordance with (1.7), the equalities

$$\varepsilon_1 + \varepsilon_2 = 0, \quad \varepsilon_3 = 0, \quad (1.16)$$

hold, and the relation (1.14) takes the form

$$I_3 = \varepsilon_x\varepsilon_y\varepsilon_z + 2\varepsilon_{xy}\varepsilon_{yz}\varepsilon_{xz} - \varepsilon_x\varepsilon_{yz}^2 - \varepsilon_y\varepsilon_{xz}^2 - \varepsilon_z\varepsilon_{xy}^2 = 0. \quad (1.17)$$

The plasticity condition

$$2\sigma_1 - \sigma_2 - \sigma_3 = \kappa, \quad (1.18)$$

which uses the maximum reduced stress (see [2]), and relations (1.10)–(1.13) turn equation (1.14) into

$$\left(\frac{I_3}{2}\right)^2 + \left(\frac{I_2}{3}\right)^3 = 0. \quad (1.19)$$

If the plasticity condition is defined as an intersection of two smooth yield surfaces

$$f_1(\sigma_{ij}) = 0, \quad f_2(\sigma_{ij}) = 0, \quad (1.20)$$

then the system of nine equations (1.1), (1.2), (1.8), and (1.20) is closed, and expressions (1.1) play the role of relations for the generalized associate law of plastic flow.

In the case of the completely plastic state, when three plasticity conditions take place, only two relations among those in (1.1) are independent [3].

2. We now consider certain linearized relations of the perfect-plasticity theory. We assume that, in the initial and strained states, the substance is homogeneous and isotropic:

$$\sigma_1^0, \sigma_2^0, \sigma_3^0, \varepsilon_1^0, \varepsilon_2^0, \varepsilon_3^0 = \text{const}. \quad (2.1)$$

The *x*-, *y*-, and *z*-axes of the Cartesian coordinate system are directed along the principal directions 1, 2, 3, respectively. Then,

$$\sigma_x^0 = \sigma_1^0, \ \sigma_y^0 = \sigma_2^0, \ \sigma_z^0 = \sigma_3^0, \ \tau_{xy}^0 = \tau_{yz}^0 = \tau_{xz}^0 = 0, \quad \varepsilon_x^0 = \varepsilon_1^0, \ \varepsilon_y^0 = \varepsilon_2^0, \ \varepsilon_z^0 = \varepsilon_3^0, \ \varepsilon_{xy}^0 = \varepsilon_{yz}^0 = \varepsilon_{xz}^0 = 0. \quad (2.2)$$

Parameters describing a perturbed state are presented as

$$\sigma_{ij} = \sigma_{ij}^0 + \sigma_{ij}', \quad \varepsilon_{ij} = \varepsilon_{ij}^0 + \varepsilon_{ij}', \quad u_i = u_i^0 + u_i'. \quad (2.3)$$

Here and below, primes mark the perturbance components.

The equilibrium equations have the form

$$\frac{\partial\sigma_x'}{\partial x} + \frac{\partial\tau_{xy}'}{\partial y} + \frac{\partial\tau_{xz}'}{\partial z} = 0,$$

$$\frac{\partial\tau_{xy}'}{\partial x} + \frac{\partial\sigma_y'}{\partial y} + \frac{\partial\tau_{yz}'}{\partial z} = 0, \quad (2.4)$$

$$\frac{\partial\tau_{xz}'}{\partial x} + \frac{\partial\tau_{yz}'}{\partial y} + \frac{\partial\sigma_z'}{\partial z} = 0.$$

It follows from relations (2.2), (2.3), and (1.1) that

$$\sigma_x' = \sigma_1', \quad \sigma_y' = \sigma_2', \quad \sigma_z' = \sigma_3', \quad \varepsilon_x' = \varepsilon_1', \quad \varepsilon_y' = \varepsilon_2', \quad \varepsilon_z' = \varepsilon_3', \quad (2.5)$$

$$\tau_{xy}' = \frac{\sigma_1^0 - \sigma_2^0}{\varepsilon_1^0 - \varepsilon_2^0}\varepsilon_{xy}', \quad \tau_{yz}' = \frac{\sigma_2^0 - \sigma_3^0}{\varepsilon_2^0 - \varepsilon_3^0}\varepsilon_{yz}', \quad \tau_{xz}' = \frac{\sigma_1^0 - \sigma_3^0}{\varepsilon_1^0 - \varepsilon_3^0}\varepsilon_{xz}'. \quad (2.6)$$

According to expressions (2.6), applied for an isotropic body, increments of principal tangential stresses and of shear rates are proportional to the initial values of these quantities.

The linearized equations of the perfect-plasticity theory make it possible to reveal the main features of the deformation process [4]. Below, we consider a plane corresponding to the Tresca plasticity condition (1.15).

According to (2.1)–(2.3) and (1.15)–(1.17), we have

$$\xi = \sigma_x' = \sigma_y', \quad (2.7)$$

$$\tau_{xy}' = \frac{\kappa}{\varepsilon_x^0}\varepsilon_{xy}', \quad \tau_{yz}' = \frac{\sigma_z^0 - \sigma_y^0}{\varepsilon_x^0}\varepsilon_{yz}', \quad \tau_{xz}' = \frac{\sigma_x^0 - \sigma_z^0}{\varepsilon_x^0}\varepsilon_{xz}', \quad (2.8)$$

$$\varepsilon_x' + \varepsilon_y' = 0, \ \varepsilon_z' = 0, \ \frac{\partial u'}{\partial x} + \frac{\partial v'}{\partial y} = 0, \ \frac{\partial w'}{\partial z} = 0. \quad (2.9)$$

Equations (2.4) and (2.7)–(2.9) yield

$$\frac{\partial\xi}{\partial x}+\frac{\kappa}{2\varepsilon_x^0}\frac{\partial}{\partial y}\left(\frac{\partial u'}{\partial y}+\frac{\partial v'}{\partial x}\right)+\frac{\sigma_x^0-\sigma_z^0}{2\varepsilon_x^0}\frac{\partial^2 u'}{\partial z^2}=0,$$

$$\frac{\partial\xi}{\partial y}+\frac{\kappa}{2\varepsilon_x^0}\frac{\partial}{\partial x}\left(\frac{\partial u'}{\partial y}+\frac{\partial v'}{\partial x}\right)+\frac{\sigma_z^0-\sigma_y^0}{2\varepsilon_x^0}\frac{\partial^2 v'}{\partial z^2}=0,$$

$$\frac{\partial\sigma_z'}{\partial z}+\frac{\sigma_x^0-\sigma_z^0}{2\varepsilon_x^0}\frac{\partial}{\partial x}\left(\frac{\partial u'}{\partial z}+\frac{\partial w'}{\partial x}\right)+\frac{\sigma_z^0-\sigma_y^0}{2\varepsilon_x^0}\frac{\partial}{\partial y}\left(\frac{\partial v'}{\partial z}+\frac{\partial w'}{\partial y}\right)=0, \tag{2.10}$$

$$\frac{\partial u'}{\partial x}+\frac{\partial v'}{\partial y}=0,\quad \frac{\partial w'}{\partial z}=0. \tag{2.11}$$

Assuming the validity of the expressions

$$u'=-\frac{\partial\Psi}{\partial y},\quad v'=\frac{\partial\Psi}{\partial x}, \tag{2.12}$$

we satisfy the incompressibility condition (2.11). Eliminating the variable ξ from the first two equations (2.10), and using (2.12), we obtain the following equation for the function Ψ:

$$\kappa\Delta\Delta\Psi+\frac{\partial^2}{\partial z^2}\left[(\sigma_z^0-\sigma_y^0)\frac{\partial^2\Psi}{\partial x^2}+(\sigma_x^0-\sigma_z^0)\frac{\partial^2\Psi}{\partial y^2}\right]=0, \tag{2.13}$$

where

$$\Delta=\frac{\partial^2}{\partial x^2}-\frac{\partial^2}{\partial y^2}.$$

It is of interest to consider the particular case

$$\sigma_z^0=\frac{1}{2}(\sigma_x^0+\sigma_y^0). \tag{2.14}$$

In this case, with allowance for (2.14), equation (2.13) takes the form

$$\Delta\Delta\Psi+\frac{\partial^2}{\partial z^2}\left[\frac{\partial^2\Psi}{\partial x^2}+\frac{\partial^2\Psi}{\partial y^2}\right]=0. \tag{2.15}$$

The case, when Ψ is independent of the z-coordinate, corresponds to plane deformation that has been considered in [4].

Under the condition of the maximum reduced stress, we have, in accordance with (1.17) and (1.18),

$$\varepsilon_x^0=-\lambda^0,\quad \varepsilon_y^0=-\lambda^0,\quad \varepsilon_z^0=2\lambda^0,$$
$$\varepsilon_x'=-\lambda',\quad \varepsilon_y'=-\lambda',\quad \varepsilon_z'=2\lambda'. \tag{2.16}$$

Equations (2.16) and (2.6) yield

$$\varepsilon_x'-\varepsilon_y'=0,\quad \varepsilon_{xy}'=0,\quad \varepsilon_x'+\varepsilon_y'+\varepsilon_z'=0. \tag{2.17}$$

In turn, (2.17) and (1.5) lead to

$$\frac{\partial u'}{\partial x}-\frac{\partial v'}{\partial y}=0,\quad \frac{\partial u'}{\partial y}+\frac{\partial v'}{\partial x}=0,$$
$$\frac{\partial u'}{\partial x}+\frac{\partial v'}{\partial y}+\frac{\partial w'}{\partial z}=0. \tag{2.18}$$

The problem of determining components of translational-velocity perturbations (2.18) is kinematically definable. With (2.12) taken into account, we obtain

$$\frac{\partial^2\Psi}{\partial x^2}+\frac{\partial^2\Psi}{\partial y^2}=0,\quad \frac{\partial\Psi}{\partial z}=-2\frac{\partial^2\Psi}{\partial x\partial y}. \tag{2.19}$$

For an edge determined by the equations

$$a_1\sigma_1+b_1\sigma_2+c_1\sigma_3=\kappa_1,$$
$$a_2\sigma_1+b_2\sigma_2+c_2\sigma_3=\kappa_2, \tag{2.20}$$
$$a_1+b_1+c_1=0,\quad a_2+b_2+c_2=0,$$

the equality

$$\sigma_x'=\sigma_y'=\sigma_z'=\sigma' \tag{2.21}$$

holds. Then, using (2.4), (2.6), (1.5), (2.21), and (1.8), we can write out the following system of equations:

$$\frac{\partial\sigma'}{\partial x}+a_{12}\frac{\partial}{\partial y}\left(\frac{\partial u'}{\partial y}+\frac{\partial v'}{\partial x}\right)+a_{13}\frac{\partial}{\partial z}\left(\frac{\partial u'}{\partial z}+\frac{\partial w'}{\partial x}\right)=0,$$

$$\frac{\partial\sigma'}{\partial y}+a_{12}\frac{\partial}{\partial x}\left(\frac{\partial u'}{\partial y}+\frac{\partial v'}{\partial x}\right)+a_{23}\frac{\partial}{\partial z}\left(\frac{\partial v'}{\partial z}+\frac{\partial w'}{\partial y}\right)=0,$$

$$\frac{\partial\sigma_z'}{\partial z}+a_{13}\frac{\partial}{\partial x}\left(\frac{\partial u'}{\partial z}+\frac{\partial w'}{\partial x}\right)+a_{23}\frac{\partial}{\partial y}\left(\frac{\partial v'}{\partial z}+\frac{\partial w'}{\partial y}\right)=0, \tag{2.22}$$

$$\frac{\partial u'}{\partial x}+\frac{\partial v'}{\partial y}+\frac{\partial w'}{\partial z}=0,$$

where

$$2a_{12}=\frac{\sigma_1^0-\sigma_2^0}{\varepsilon_1^0-\varepsilon_2^0},\quad 2a_{23}=\frac{\sigma_2^0-\sigma_3^0}{\varepsilon_2^0-\varepsilon_3^0},\quad 2a_{13}=\frac{\sigma_1^0-\sigma_3^0}{\varepsilon_1^0-\varepsilon_3^0}.$$

In all cases of static indeterminacy, the above-considered equations are of the elliptic type. Linearized equations for statically definable states of a perfectly plastic body have been considered in [5].

REFERENCES

1. A. Yu. Ishlinskiĭ, Uchen. Zap. Mos. Gos. Univ., Ser. Mekh., No. 117, 90 (1946).
2. A. Yu. Ishlinskiĭ, Uchen. Zap. Mos. Gos. Univ., Ser. Mekh., No. 46, 117 (1940).
3. D. D. Ivlev, Dokl. Akad. Nauk **361**, 765 (1998) [Dokl. Phys. **43**, 509 (1998)].
4. A. Yu. Ishlinskiĭ, Dokl. Akad. Nauk Ukr. SSR, No. 1, 12 (1958).
5. L. A. Maksimova, Dokl. Akad. Nauk **358**, 772 (1998) [Dokl. Phys. **43**, 131 (1998)].

Translated by Yu. Verevochkin

Doklady Physics, Vol. 45, No. 3, 2000, pp. 118–121. Translated from Doklady Akademii Nauk, Vol. 371, No. 2, 2000, pp. 182–185.

MECHANICS

On Dynamic Materials

I. I. Blekhman* and K. A. Lurie**

Presented by Academician K.V. Frolov May 20, 1999

Received May 25, 1999

In this study, we propose an idea of creating dynamic materials by which we mean the media composed of regular materials distributed in space and time. An important class of such structures, which are distributed only in space at a microscale, is a class of standard composites. The appearance of time as a supplementary and, as a rule, fast-varying independent variable converts such materials into dynamic composites, i.e., into space–time formations.

Properties of dynamic materials can be substantially different from those of their constituent initial materials. By varying material parameters of the initial components and the character of changing these parameters in time, we can control the dynamic properties of these materials and obtain some effects impossible when using regular materials.

The aforesaid refers not only to mechanical materials characterized by the inertial, elastic, dissipative, and other parameters, but also to electrotechnical materials, whose principal characteristics are the self-inductance, the capacitance, etc. Important principal aspects of this problem are also associated with taking into account relativistic effects [1–3]. However, in this paper, we shall restrict our consideration only to classical mechanical materials.

1. TWO TYPES OF DYNAMIC MATERIALS

Two methods for obtaining dynamic materials and two types of such materials, respectively, are conceivable.

The first-type materials are obtained by instantaneous or gradually changing the material parameters of various parts of a system (masses, rigidities, self-inductance, capacitance, etc.) with no relative motion of these parts. Such a method is termed the *activation* [2, 3], and the corresponding materials are called the *dynamic materials of the first type or activated dynamic materials*.

In the second method, the entire system or its certain parts are presumed to be set in motion, which is predetermined or excited by a certain method. Such a method will be conventionally called the *kinetization*, and the corresponding materials will be called the *dynamic materials of the second type or kinetic dynamic materials*.

In particular, a dynamic material of the second type can be imagined in the form of two or several mutually penetrating media occupying a certain domain of space, with each medium accomplishing a particular motion (for example, fast vibrations) with respect to others. It is natural that material parameters and properties of such a material can be substantially different from those of the initial media. There are considerable opportunities for controlling these properties.

2. ON A TECHNICAL REALIZATION OF DYNAMIC MATERIALS

The natural question arises about the possibilities for the technical realization of the dynamic materials described. As to the materials of the first type, the corresponding methods are known for the electrotechnical materials. Therefore, we dwell here on certain methods for realizing the dynamic materials of the second type. In Fig. 1, we show the system consisting of plates adjacent to one another. Every plate is set in periodic vibrations

$$u(x_s, t) = u(x_s, t + T_s)$$

with the period T_s depending on the coordinate x_s (the number of a plate). The density, the elastic modulus, or other material parameters, as well as the thickness of each plate, can be distributed in a certain way along the length of the plate (z-coordinate). In Fig. 1, the one-dimensional case, when material properties vary "rapidly" along the x-coordinate, is shown. However, a more complicated two-dimensional variant of this scheme is also conceivable. The variant, which is sim-

* *Institute of Problems in Machine Science, Russian Academy of Sciences, Vasil'evskiĭ ostrov, Bol'shoĭ pr. 61, St. Petersburg, 199178 Russia*
e-mail: blekhman@vibro.ipme.ru

** *Worcester Polytechnical Institute, 100 Institute Road, Worcester, MA 01609, USA*
e-mail: klurie@wpi.edu

1028-3358/00/4503-0118$20.00

pler for realization, corresponds to all odd plates and all even plates moving identically, i.e.,

$$u(t, x_1) = u(t, x_3) = \ldots = u(t, x_{2n-1}),$$
$$u(t, x_2) = u(t, x_4) = \ldots = u(t, x_{2n}).$$

In this case, each of the odd plates can be adjoined to a certain vibrating solid, and each of the even plates, to another solid.

In Fig. 2, we present the scheme of the system in which the odd circular disks are fixed at a certain shaft, while the even disks are attached to another shaft. The shafts can rotate with certain angular velocities ω_1 and ω_2 or accomplish rotary vibrations with the frequencies ω_1 and ω_2 and with the angular amplitudes Φ_1 and Φ_2. Parameters of the plate's material can depend on the angular coordinates φ_1 and φ_2 and, of course, on the number of a plate. In this case, the one-dimensional medium with variable material parameters is a rod with the x-axis and a lens-shaped cross section. Using the disks with more complicated shapes (see, for example, dashed curves in Fig. 2) instead of the circular ones with identical radii, it is also easy to obtain the cross-section area of the rod which is variable along the x-coordinate and in time. One can also envision an even more complicated case when each disk is fixed at its own shaft and vibrates or rotates according to its own law.

In Fig. 3, we show a vessel completely filled with a liquid of certain density ρ_0, elasticity E_0, viscosity μ, and with other certain material parameters. In this vessel, balls with different diameters d_s (which are small as compared with the vessel dimension), densities ρ_s, and other material parameters are distributed in a particular way. The vessel is set in periodic vibrations in one, two, or three directions. In this case, it is known that the balls will vibrate with amplitudes substantially dependent on the ball dimension and density [4, 5]. Choosing, in a certain way, these parameters and the concentrations of the balls in the vessel, we obtain a medium, whose effective properties vary along one, two, or three coordinates. The balls can be deformable (for example, rubber capsules filled with air), and in this case, resonance effects can be employed. For preserving the medium properties when vibrations are discontinued for a while, the balls can be bound by elastic elements providing a particular arrangement of the balls in the static position and also, possibly, the resonance effects when the vessel vibrates. A homogeneous suspension is the simplest version of the medium described. In this case, the liquid is one of the mutually penetrating media, while the set of particles forming the suspension is the other one. Instead of the balls, bodies with a more complicated shape can be used. Effective properties of the media described can be determined using the methods outlined in book [6] and report [10].

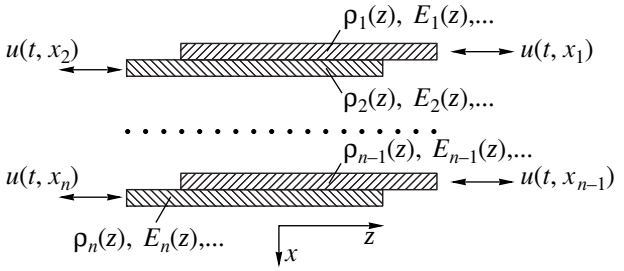

Fig. 1.

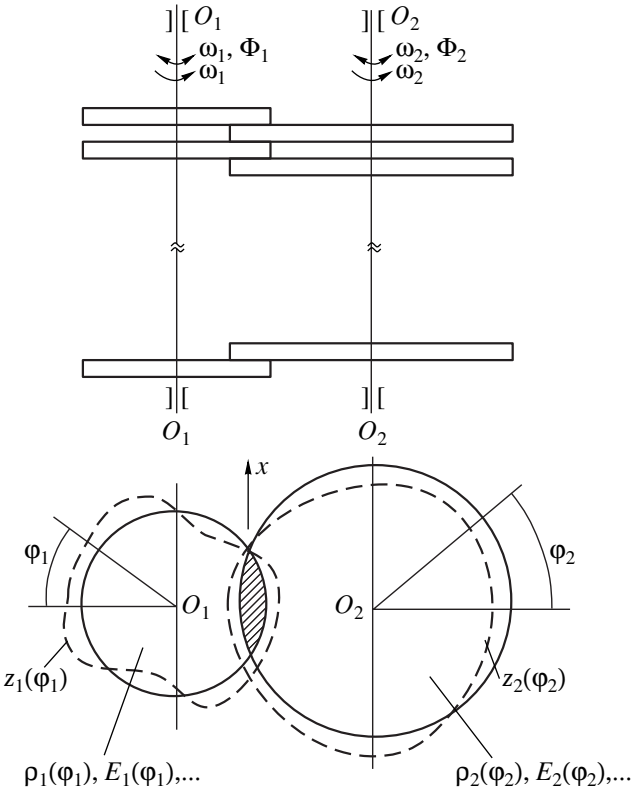

Fig. 2.

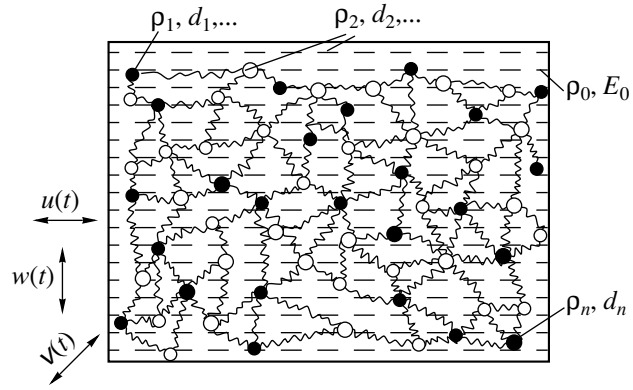

Fig. 3.

3. ON THE POSSIBILITIES PROVIDED BY THE USE OF DYNAMIC MATERIALS

Certain possibilities provided by using the dynamic materials can be illustrated by the simplest example. We consider a rod, whose effective density ρ, elastic modulus E, and cross-section area F can be specified in the form of functions of the x-coordinate, measured along the rod axis, and the time t. The motion of such a rod is described by the equation

$$(\varphi u_t)_t = (\psi u_x)_x, \quad (1)$$

where $\psi = \psi(x, t) = E(x, t)F(x, t)$, $\varphi = \varphi(x, t) = \rho(x, t)F(x, t)$, and the subscripts t and x denote the corresponding partial derivatives.

It is proposed to provide the required motion $u(x, t)$ of the rod through the proper choice of the functions ρ, E, and F (and, of course, the initial conditions); i.e., this is a peculiar inverse problem of mechanics.

The solution to equation (1) depends on two functions φ and ψ, both of them entering the equation completely symmetrically. If the function ψ is given, it is easy to find from this equation:

$$\varphi = \frac{1}{u_t}\int(\psi u_x)_x dt. \quad (2)$$

For a given φ, the function ψ can be determined by the same equality by substituting ψ for φ, t for x, and x for t.

Two particular cases are of interest for which expression (2) can be further simplified.

(1) The function $u(x, t)$ is given in the form of a product

$$u(x, t) = u_1(t)u_2(x)$$

or in the form of the sum of such products. In this case, it is natural to seek the functions φ and ψ in the same form:

$$\varphi(x, t) = \varphi_1(t)\varphi_2(x), \quad \psi(x, t) = \psi_1(t)\psi_2(x).$$

In this case, the variables in equation (1) can be separated, and we find

$$\varphi_1 = \frac{\lambda}{(u_1)_t}\int\psi_1 u_1 dt, \quad \varphi_2 = \frac{1}{\lambda}\frac{[\psi_2(u_2)_x]_x}{u_2},$$

$$\psi_1 = \frac{1}{\lambda}\frac{[\varphi_1(u_1)_t]_t}{u_1}, \quad \psi_2 = \frac{\lambda}{(u_2)_x}\int\varphi_2 u_2 dx,$$

where λ is a constant. From these formulas, any two functions can be determined if two others are given.

(2) The function $u(x, t)$ is given in the form

$$u(x, t) = u(x - vt),$$

i.e., in the form of a wave traveling with a certain velocity v.

In this case, it is natural to seek the functions φ and ψ also in the form of traveling waves ("waves of properties")

$$\varphi(x, t) = \varphi(x - vt), \quad \psi(x, t) = \psi(x - vt),$$

and from equation (1), we obtain the ordinary differential equation

$$v^2(\varphi u')' = (\psi u')'$$

with the independent variable $z = x - vt$ (the prime denotes differentiating with respect to this variable). From this equation, it is easy to determine one of the functions φ or ψ if the other is known.

As was shown in papers [1–3], under certain conditions, it is possible to isolate completely a certain part of a body from long-wave disturbances by activating a dynamic material through the organization of the "wave of properties".

4. ON DYNAMIC SURFACES

It should be noted that two-dimensional analogs of proposed dynamic materials (they can be called dynamic surfaces) are known. Remarkable dynamic properties manifested by these surfaces serve as further corroboration of significant technical potentialities provided by the use of dynamic materials. However, it is worth noting that the indicated surfaces have never been mentioned as being dynamic materials. We outline three indicated systems.

The first of them is a plane formed by two systems of alternating parallel fibers. The fibers of the first system (assume, for example, that they are the odd fibers) move in a certain direction, while the fibers of the other system (the even fibers) move with the same velocity in the opposite direction. It is easy to see that a reasonably extended body lying on such a surface will be under the action of the viscous-friction-type forces, whereas the friction between an individual fiber and the body is of the dry type (the Coulomb-type) [7, 8].

Another example is a surface formed by two identical parallel horizontal rollers rotating with identical angular velocity in opposite directions. A linear "elastic" restoring force acts on a body placed on such rollers. In other words, the body behaves as a conservative linear oscillator in spite of the fact that the forces of dry friction act between the body and the surface of the rollers [7, 8].

A plane formed by two groups of alternating rods can serve as the third example. The rods of the first group (assume that they are the odd rods) are attached to a certain solid, while the rods of the second group, to another solid. These solids each execute given translation vibrations along certain trajectories [9]. Under certain conditions, a sufficiently extended body placed on such a plane experiences impact and force actions with a nonzero mean component; this is unattainable or is not easily attainable using a continuous vibrating

plane [9, 10]. This fact makes it possible to obtain a significant technological effect in systems for transporting and sifting bulk materials.

Needless to say, the realization of the idea of dynamic material is more complicated in the three-dimensional case and requires special technical solutions; here, we presented the concepts of three such solutions. Moreover, such solutions are the subject for patenting. One of the concerns of this work was to initiate the appearance of these solutions.

ACKNOWLEDGMENTS

I. I. Blekhman thanks the Russian Foundation for Basic Research for support of his work (grant no. 99-01-00721). K. A. Lurie thanks the National Science Foundation (USA) (grant no. DMS 9803476), and the Fulbright Foundation for support of his work.

REFERENCES

1. K. A. Lurie, J. Struct. Solids **34**, 1633 (1997).
2. K. A. Lurie, Proc. Roy. Soc. (London) **A454**, 1767 (1998).
3. K. A. Lurie, Control and Cybernetics **27**, 283 (1998).
4. N. L. Granat, Izv. Acad. Nauk SSSR, Ser. Mekh. and Mashinostr., No. 1, 70 (1960).
5. N. L. Granat, Izv. Acad. Nauk SSSR, Ser. Mekh. and Mashinostr., No. 5, 61 (1964).
6. I. I. Blekhman, *Vibrational Mechanics* (Fizmatlit, Moscow, 1994).
7. Ya. G. Panovko and I. I. Gubanova, *Stability and Vibrations in Elastic Systems* (Nauka, Moscow, 1979).
8. S. P. Timoshenko, *Vibrations in Engineering* (Fizmatgiz, Moscow, 1959).
9. I. I. Blekman and G. B. Bukaty, Izv. Akad. Nauk SSSR, Ser. Mekh. Tverd. Tela **2**, 36 (1975).
10. I. I. Blekhman, in *Proceedings of Symp. Synthesis of Nonlinear Dynamical Systems*, Riga, 1998.

Translated by V. Bukhanov

Doklady Physics, Vol. 45, No. 3, 2000, pp. 122–124. Translated from Doklady Akademii Nauk, Vol. 371, No. 2, 2000, pp. 186–188.

MECHANICS

Nonmonotone Time Dependence of Dynamic Fracture Viscosity of Solids

Corresponding member of the RAS N. F. Morozov, Yu. V. Petrov, and V. V. Taraban

Received October 22, 1999

Testing the strength properties of different materials implies a choice of reliable parameters being measured that characterize the fracture. For example, in analysis of the dynamic fracture of materials containing cracks, a concept of the dynamic fracture viscosity is widely used. This quantity is assumed to be the intrinsic characteristic of the material, and its time dependence (before the fracture has occurred) corresponds to a steadily decreasing function. An empirical formula for this dependence was proposed in [1]:

$$K_{Id} = K_{Is} + \frac{C}{t_c^2}.$$

Here, K_{Id} and K_{Is} are dynamic and static fracture viscosities, respectively, and t_c is the time lapse before fracturing. However, the experimental data demonstrate a possibility of a nonclassic (nonmonotone) behavior of the dynamic fracture viscosity for some materials under specific conditions of their loading. In [2], this effect is related to only variations in mechanical properties for the materials under an intense high-rate loading (a passage to the viscoelastic state). The rheological models describing such a behavior are rather complicated and nonuniversal, and hence they are hardly applicable to actual calculations of strength characteristics. The dependence of the parameters characterizing the static fracture (the fracturing stress and the crack strength limit) on the typical size of cracks existing in the material was revealed in [3]. We can also expect the existence of a certain relationship between the characteristics of dynamic fracture and the crack size in the case of the dynamic loading.

As a test example, we consider a problem where the normal pressure $\sigma_{zz} = -\sigma H(t)$ is suddenly applied to the surface of the disk-shape crack with the radius R, which is located within the homogeneous isotropic elastic space. Here, σ is a constant factor and $H(t)$ is the Heaviside step function.

St. Petersburg State University, Universitetskaya nab., St. Petersburg, 199164 Russia

We now use certain explicit results reported in [4]. Then, the stress intensity factor can be written in the form

$$K_I(t') = k_I \int_0^{t'} \varphi(1, s)\,ds, \tag{1}$$

where $k_I = \sigma\frac{\sqrt{2R}}{\pi}$ is the stress intensity factor for the corresponding static problem, $t' = t/T$ is the dimensionless time. Here, $T = R/c_2$ is the characteristic time of the problem (the time for a wave to pass by the distance equal to the crack radius) and c_2 is the transverse wave velocity. The Laplace transform of the function

$$\Phi(1, p) = \int_0^{+\infty} \varphi(1, t)e^{-pt}dt, \tag{2}$$

can be found as a solution to the Fredholm integral equation

$$\Phi(\eta, p) = \eta + \int_0^1 \Phi(\xi, p)H(\xi, \eta)\,d\xi, \quad 0 \le \xi, \eta \le 1, \tag{3}$$

with the kernel

$$H(\xi, \eta) = h(\xi, \eta) + \frac{2p}{\pi}\int_0^{+\infty} \omega(x)\sin(\xi px)\sin(\eta px)\,dx.$$

Here, we use the following notation

$$h(\xi, \eta) = \frac{Mp}{2m}(e^{-|\xi-\eta|mp} - e^{-(\xi+\eta)mp}),$$

$$\omega(x) = 1 + \frac{M}{x^2 + m^2} - \frac{2}{1-\theta^2} \times \frac{(x^2 + 0.5)^2 - x^2\sqrt{(x^2+1)(x^2+\theta^2)}}{x\sqrt{x^2+\theta^2}},$$

1028-3358/00/4503-0122$20.00

$$M = \frac{3-4\theta^2+3\theta^4}{4(1-\theta^2)}, \quad m = \frac{1+2\theta^2-6\theta^4+5\theta^6}{8M(1-\theta^2)},$$

$$\theta = \frac{c_2}{c_1} = \sqrt{\frac{1-2\nu}{2-2\nu}},$$

where ν is the Poisson's ratio and c_1 is the velocity of longitudinal waves.

Integral equation (3) was solved numerically with the use of the Simpson integration formulas and the Gauss exclusion method. The numerical inversion of the Laplace transform (2) can be performed by using the Bellman matrices, the corresponding technique is described in the monograph [5].

We have calculated the dependence of the stress intensity coefficient on the dimensionless time substituting the original $\varphi(1, s)$ into (1). This dependence plotted for different values of the Poisson's ratio (ν = 0.09, 0.29, and 0.49) is shown in Fig. 1.

We assume furthermore that the fracture occurs according to the elastic–fragile scenario (i.e., the material retains its elastic properties until the fracture has occurred). The analysis of the strength and fracture is performed on the basis of the structure-time criterion [6]

$$\int_{t-\tau}^{t} K_I(s)ds \le K_{Is}\tau. \qquad (4)$$

Here, τ is the structural time for fracturing. We calculate the dynamic fracture viscosity (the critical value of the coefficient for stress intensities initiating fracturing the material at a time t_c)

$$K_{Id} = K_I(t_c') = \sigma_c\frac{\sqrt{2R}}{\pi}\int_0^{t_c'}\varphi(1, s)ds.$$

Here, $t_c' = t_c/T$ and σ_c is the minimum load leading to fracturing. This load is determined by substituting (1) into (4) under the condition of equality attained in (4). Introducing the notation $f(t') = \int_0^{t'}\varphi(1, s)ds$, we find eventually the following expression for the dynamic fracture viscosity

$$K_{Id} = K_{Is}\left[\frac{T}{\tau}\int_{(t_c-\tau)/T}^{t_c/T}\frac{f(s)}{f(t_c')}ds\right]^{-1}. \qquad (5)$$

The crack size is involved here into T and t_c'.

The dependence of the dynamic fracture viscosity calculated according to (5) on the time elapsed before the fracture has appeared is shown in Fig. 2 for the case of a high-strength steel (ν = 0.29, τ = 7 μs, c_1 = 6 mm/μs, and K_{Is} = 47 MPa$\sqrt{\text{m}}$) at different values of the parameter T/τ. We can distinguish three qualitatively different types of the behavior for the dynamic fracture viscosity at different values of T/τ.

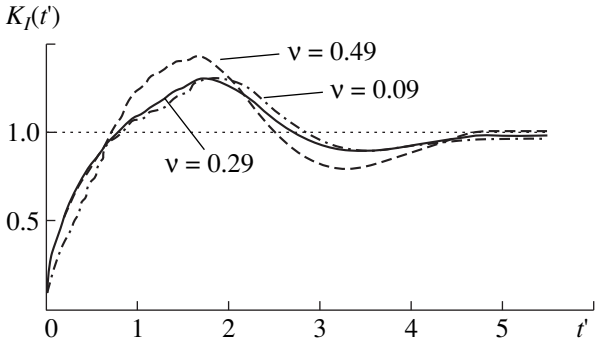

Fig. 1. Stress-intensity coefficient as a function of dimensionless time at different values of the Poisson's ratio.

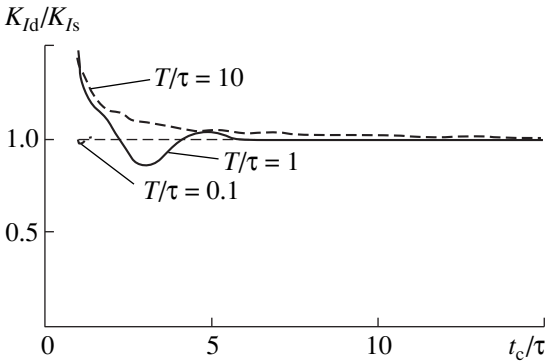

Fig. 2. Dynamic fracture viscosity as a function of time elapsed before fracturing high-strength steel at different values of the ratio T/τ.

(i) If the ratio T/τ is sufficiently small (we have considered the case of T/τ = 0.1, which corresponds to R = 2.5 mm), then the oscillations of the dynamic fracture viscosity are negligible and decay rapidly, i.e., the fracture of the material exhibits a quasi-static behavior.

(ii) When the characteristic time T of the problem is comparable with the structural time of the fracture (the case of T/τ = 1 corresponding to R = 25 mm is considered), we observe the significant nonmonotonicity of the dynamic fracture viscosity since the initial oscillations of K_{Id} are rather pronounced. Such a dependence of the dynamic fracture viscosity on the time elapsed before the fracture agrees qualitatively and coincides (on the order of magnitude) with the similar nonmonotone experimental curve reported in [2]. The tests were performed for a sample of the high-strength steel with the same mechanical properties and containing the crack of the same size as was discussed above.

(iii) With increasing the ratio T/τ, the nonmonotonicity of the dynamic fracture viscosity gradually disappears. If the characteristic time T of the problem much exceeds the structural time for fracturing (we

have considered the case $T/\tau = 10$ corresponding to $R = 250$ mm), then the behavior of dynamic fracture viscosity is nearly indistinguishable from the classical behavior observed in experiments for sufficiently long cracks (see, e.g., [1]).

We may conclude that the nonclassic (nonmonotone) diagrams of the dynamic fracture viscosity were obtained in this study in accordance with the elastic-fragile fracture scenario for a material. It was shown that these diagrams are related to the effect of the crack size on the dynamic fracture viscosity. Hence, it follows that the dynamic fracture viscosity depends not only on the mechanical properties of the material but on the geometry parameters of a specific problem as well.

REFERENCES

1. K. Ravi-Chandar and W. G. Knauss, Int. J. Fracture **25**, 247 (1984).
2. J. F. Kalthoff, Eng. Fract. Mech. **23**, 289 (1986).
3. Yu. V. Petrov and V. V. Taraban, Vestn. St. Petersb. Univ., Ser. 1, No. 2, 78 (1997).
4. P. A. Martynyuk, in *Dynamics of Continuum*, No. 25, 82 (1974).
5. R. Bellman, R. Kalaba, and J. Lockett, *Numerical Inversion of the Laplace Transform* (Amsterdam, 1966).
6. Y. V. Petrov and N. F. Morozov, ASME J. Appl. Mech. **61**, 710 (1994).

Translated by K. Kugel'

Doklady Physics, Vol. 45, No. 3, 2000, pp. 125–128. Translated from Doklady Akademii Nauk, Vol. 371, No. 3, 2000, pp. 329–332.

MECHANICS

A Criterion of Stability in the Lyapunov Sense for a Family of Periodic Solutions

O. V. Druzhinina

Presented by Academician V.V. Rumyantsev July 7, 1999

Received July 14, 1999

A criterion of stability in the Lyapunov sense, which is established here, concerns a family of periodic solutions depending on many independent parameters. The solutions relate to a $(n + k)$-dimensional system of time-independent differential equations of the following vector form:

$$\dot{x} = g(x), \quad g(x) = (g_1(x), \ldots, g_{n+k}(x)). \tag{1}$$

Here, $x = (x_1, \ldots, x_{n+k}) \in J \subset R^{n+k}$ and, in the set J, the function g: $J \longrightarrow R^{n+k}$ has continuous second order partial derivatives with respect to components of the vector $x \in R^{n+k}$.

The following holds true:

Theorem 1. *Let the following conditions hold*: (i) *The differential system* (1) *has the family of* ω*-periodic solutions*

$$x_s = \varphi_s(t, h_1, \ldots, h_k), \quad s = 1, \ldots, n + k, \tag{2}$$

which depend on k independent parameters ($k \geq 1$) *belonging to the set* $B = \{h \in R^k, |h| \leq r\}$. (ii) *The system of variational equations*

$$\dot{y} = \frac{\partial g}{\partial x}(\varphi_s(t, h_1, \ldots, h_k))y, \quad y \in R^{n+k}, \tag{3}$$

has $k + 1$ *zero characteristic exponents and* $n - 1$ *characteristic exponents with negative real-valued parts.*

Then, at sufficiently small values of $|h_1|, \ldots, |h_k|$, *each solution of family* (2) *is stable in the Lyapunov sense if and only if the period* ω *of family* (2) *is independent of the parameters* $h_1, \ldots, h_k$.

Remark. The condition of Theorem 1 for existence of $k + 1$ zero characteristic exponent is met automatically (see [1, 2]).

Proof. Necessity. Let, at sufficiently small values of $|h_1|, \ldots, |h_k|$, each solution of family (2) be stable in the Lyapunov sense. Assume further that $\frac{\partial \omega}{\partial h_k} \neq 0$, i.e., the parameter h_k is a period of functions (2). The change of variables $t \longrightarrow t\omega^{-1}$ turns (1) into the system

$$\omega\dot{x} = g(x), \quad x \in R^{n+k}, \tag{4}$$

having 2π-periodic solutions. Let the set $(\sigma, \psi(t))$ be a solution to the following variational system for (4):

$$\sigma\dot{y} = \frac{\partial g}{\partial x}(\psi(t))y, \quad y \in R^{n+k}. \tag{5}$$

We denote the fundamental matrix of solutions to (5) by $Y(t)$. It is the solution to the matrix differential equation

$$\sigma\dot{Y}(t) = \frac{\partial g}{\partial x}(\psi(t))Y(t), \quad Y(0) = E, \tag{6}$$

where E is a unit matrix of the order $(n + k)$. Unity represents the eigenvalue of the matrix $Y(2\pi)$ with the multiplicity $(k + 1)$.

As is known [2], the necessary condition concerning the stability of the solution in the first approximation lies in the fact that the Jordan block corresponding to the unit eigenvalue is diagonal, i.e., there are $k + 1$ independent eigenvectors corresponding to unity. If this is not the case, there is the nonzero vector $y_1(0)$ satisfying the relations

$$[E - Y(2\pi)]y_1(0) \neq 0, \quad [E - Y(2\pi)]^2 y_1(0) = 0. \tag{7}$$

Relations (7) hold because $Y(2\pi)$ has a nontrivial proper subspace corresponding to unity.

Let $y_1 = \frac{\partial \psi(t)}{\partial h_i}$, where $\frac{\partial \psi}{\partial h_i} \neq 0$. Then, the function $y_1(t)$ will satisfy the equation

$$\sigma\dot{y}_1 = \frac{\partial g}{\partial x}(\psi(t))y_1 - \frac{1}{\sigma}\frac{\partial \sigma}{\partial h_i}\dot{\psi}(t), \tag{8}$$

because (8) represents the result of differentiation of system (5) with respect to h_i.

Russian State Open Technical University of Communications, ul. Chasovaya 22/2, Moscow, 125808 Russia

1028-3358/00/4503-0125$20.00

Relation (8) is a linear nonhomogeneous equation with respect to y_1. The latter quantity can be expressed as

$$y_1(t) = Y(t)\left[y_1(0) - \frac{1}{\sigma}\frac{\partial\omega}{\partial h_i}\int_0^t Y^{-1}(\tau)\dot{\psi}(\tau)d\tau\right]. \quad (9)$$

Since the derivative $\dot{\psi}(t)$ represents a solution to system (5), $\dot{\psi}(t) = Y(t)\dot{\psi}(0)$ or $Y^{-1}(t)\dot{\psi}(t) = \dot{\psi}(0)$. Substituting the obtained relation into (9) yields

$$y_1(t) = Y(t)\left[y_1(0) - \frac{1}{\sigma^2}\frac{\partial\sigma}{\partial h_i}\dot{\psi}(0)t\right],$$

or

$$[E - Y(2\pi)]y_1(0) = -\frac{2\pi}{\sigma^2}\frac{\partial\sigma}{\partial h_i}\dot{\psi}(0). \quad (10)$$

Since $\dot{\psi}(0) \neq 0$, $y_1(0) \neq 0$. Moreover, the equality $Y(2\pi)\dot{\psi}(0) = \psi(0)$ leads to the relation $[E - Y(2\pi)]^2 y_1(0) = 0$.

Solution (2) is unstable in the Lyapunov sense. Because of the contradiction obtained, the assumption that one of the parameters h_k represents the period is false.

Let, at sufficiently small values of $|h_1|, \ldots, |h_k|$, the period ω of family (2) be independent of the parameters.

We take the solution $\varphi_i(t, 0, \ldots, 0)$ to system (1) as an unperturbed one and assume that the perturbations $y_i = x_i - \varphi_i(t, 0, \ldots, 0)$ satisfy the equations for perturbed motion

$$\frac{dy_i}{dt} = \sum_{j=1}^{n+k} P_{ij}(t)y_j + Y_i(t, y_1, \ldots, y_{n+k}), \quad i = 1, \ldots, n+k. \quad (11)$$

Here, $P_{ij}(t) = \dfrac{\partial g_i(\varphi_s(t, 0, \ldots, 0))}{\partial x_j}$ and Y_i are the functions of the second order of smallness with respect to the components y_i. The functions P_{ij} and Y_i are ω-periodic in t.

We consider the variational system

$$\frac{dy_i}{dt} = \sum_{j=1}^{n+k} P_{ij}(t)y_j, \quad i = 1, \ldots, n+k. \quad (12)$$

Since system (1) admits solution (2), the differential system (11) has the solution $\psi_i = \varphi_i(t, h_1, \ldots, h_k) - \varphi_i(t, 0, \ldots, 0)$, which depends as well on k arbitrary parameters. This solution can be written as

$$\psi_i = \sum_{j=1}^{k}\left(\frac{\partial\varphi_i}{\partial h_j}\right)_0 h_j + \Psi_i(t, h_1, \ldots, h_k), \quad i = 1, \ldots, n+k. \quad (13)$$

Here, the functions Ψ_i are ω-periodic in t and are of the second (or higher) order of smallness with respect to h_j.

As a result, the variational system (12) has the family of periodic solutions of the form

$$\varphi_i^* = \sum_{j=1}^{k}\left(\frac{\partial\varphi_i}{\partial h_j}\right)_0 h_j, \quad i = 1, \ldots, n+k, \quad (14)$$

depending on k arbitrary parameters. Therefore, the variational system (12) has $k + 1$ characteristic exponents with zero real-valued parts. We assume that real-valued parts of the other characteristic exponents are nonzero. According to A.M. Lyapunov, even if one of the characteristic exponents has a positive real-valued part, the periodic solution under investigation is always unstable.

If real-valued parts of $n - 1$ characteristic exponents are negative, the issue of stability cannot be solved based on variational equations, because the other $k + 1$ exponents have zero real-valued parts. However, in the case under consideration, if differential system (12) has $n - 1$ characteristic exponents with negative real-valued parts, then, at sufficiently small values of $|h_i|$, $i = 1, \ldots, k$, both the unperturbed solution and solutions (14) are stable in the Lyapunov sense. Moreover, each perturbed solution that is sufficiently close to the unperturbed one, approaches one of the periodic solutions (2).

Indeed, a linear real-valued transformation that contains a periodic matrix and has an inverse transformation with the same properties allows differential system (12) to be reduced to a linear system with a constant matrix. In addition, the characteristic equation of this system has $n - 1$ and $k + 1$ roots with negative and zero real-valued parts, respectively.

Differential system (12) has a periodic solution with k arbitrary parameters, and coefficients of the transformation are periodic functions of the same period. Therefore, the system with a constant matrix must have k independent solutions consisting of either constants or ω-periodic functions. These solutions can be related only to those roots of the characteristic equation which have zero real-valued parts. Moreover, all of these roots are equal to either $\pm 2\pi i/\omega$ or zero. To be specific, we assume that the characteristic equation of the system with a constant matrix has the zero root of the multiplicity m_1 and imaginary roots equal to $\pm 2\pi i/\omega$ of the multiplicity m_2, where $m_1 + 2m_2 = k$. The solutions corresponding to these roots must be free from secular terms. Therefore, each such root causes both the determinant of the characteristic equation and its minors to

vanish, and the orders that do not exceed the root multiplicity are lowered by unity. Consequently, using a linear transformation with a constant matrix allows system (12) to be transformed into

$$\frac{du_i}{dt} = 0, \quad i = 1, 2, \ldots, m_1, \quad \frac{dv_j}{dt} = \frac{2\pi}{\omega}w_j,$$
$$\frac{dw_j}{dt} = \frac{2\pi}{\omega}v_j, \quad j = 1, \ldots, m_2,$$
$$\frac{dz_s}{dt} = a_{s1}z_1 + \ldots + a_{sn}z_n, \quad s = 1, \ldots, n,$$

where u_i, v_j, w_j, and z_s are new variables, and a_{si} are constants such that the roots of the equation

$$|A - \lambda E| = 0, \quad A = \|a_{si}\|, \tag{15}$$

have negative real-valued parts. In the new variables, the family of periodic solutions (14) of system (12) has the following form:

$$u_i^* = \alpha_i, \quad i = 1, 2, \ldots, m_1,$$
$$v_j^* = \beta_j\cos\frac{2\pi}{\omega}t + \gamma_j\sin\frac{2\pi}{\omega}t,$$
$$u_j^* = -\beta_j\sin\frac{2\pi}{\omega}t + \gamma_j\cos\frac{2\pi}{\omega}t, \quad j = 1, \ldots, m_2, \tag{16}$$
$$z_1^* = \ldots = z_n^* = 0.$$

Here, α_i, β_j, and γ_j are constants. Consequently, in the new variables, the periodic solution (13) to the system of equations describing the perturbed solution (11) can be written as

$$\bar{u}_i = \alpha_i + U_i(t, \alpha_1, \ldots, \alpha_{m_1}, \beta_1, \ldots, \beta_{m_2}, \gamma_1, \ldots, \gamma_{m_2}),$$
$$i = 1, \ldots, m_1,$$
$$\bar{v}_j = \beta_j\cos\frac{2\pi}{\omega}t + \gamma_j\sin\frac{2\pi}{\omega}t + V_j(t, \alpha_1, \ldots, \alpha_{m_2}),$$
$$\bar{w}_j = -\beta_j\sin\frac{2\pi}{\omega}t + \gamma_j\cos\frac{2\pi}{\omega}t + W_s(t, \alpha_1, \ldots, \alpha_{m_2}), \tag{17}$$
$$j = 1, \ldots, m_2,$$
$$\bar{z}_s = Z_s(t, \alpha_1, \ldots, \alpha_{m_2}), \quad s = 1, \ldots, n.$$

Here, U_i, V_j, W_j, and Z_s are the functions of the corresponding variables and have a second (or higher) order of smallness with respect to them. They are ω-periodic functions in t.

The substitutions

$$u_i = y_i + U_i(t, y_1, \ldots, y_{m_1}, y_{m_1+1}, \ldots, y_{m_2+m_2},$$
$$y_{m_1+m_2+1}, \ldots, y_k), \quad i = 1, \ldots, m_1,$$
$$v_j = y_{m_1+j}\cos\frac{2\pi}{\omega}t$$
$$+ y_{m_1+m_2+j}\sin\frac{2\pi}{\omega}t + V_j(t, y_1, \ldots, y_k), \tag{18}$$
$$w_j = -y_{m_1+j}\sin\frac{2\pi}{\omega}t$$
$$+ y_{m_1+m_2+j}\cos\frac{2\pi}{\omega}t + W_j(t, y_1, \ldots, y_k), \quad j = 1, \ldots, m_2,$$
$$z_s = x_s + Z_s(t, y_1, \ldots, y_k), \quad s = 1, \ldots, n$$

transform (11) into the following differential system:

$$\frac{dx_s}{dt} = a_{s1}x_1 + \ldots + a_{sn}x_n$$
$$+ X_s(t, y_1, \ldots, y_k, x_1, \ldots, x_n), \quad s = 1, \ldots, n, \tag{19}$$
$$\frac{dy_j}{dt} = Y_j(t, y_1, \ldots, y_k, x_1, \ldots, x_n), \quad j = 1, \ldots, k.$$

The system obtained has the solution $y_1 = c_1, \ldots, y_k = c_k$, $x_1 = \ldots = x_n = 0$, where c_j are arbitrary constants. Therefore, the functions X_s and Y_j must vanish at $x_1 = x_2 = \ldots = x_n = 0$.

All of the transformations used are such that the problem of stability with respect to the original variables is equivalent to that with respect to the new variables. Consequently, the problem under consideration is reduced to the investigation of the zero solution $y_1 = \ldots = y_k = x_1 = \ldots = x_n = 0$ to differential system (19), which was studied by Lyapunov in the case when real-valued parts of the roots of equation (15) were negative. According to Lyapunov, both the unperturbed solution and all of the solutions $y_1 = c_1, \ldots, y_k = c_k$ that are sufficiently close to the former are stable. Moreover, at sufficiently small perturbations, each perturbed solution tends asymptotically to one of those mentioned above as $t \longrightarrow +\infty$. Going over to the original variables allows the following conclusions to be formulated: At sufficiently small absolute values of $h_1, \ldots, h_k$, the solution $\varphi_i(t, 0, \ldots, 0)$ and all of the solutions $\varphi_i(t, h_1, \ldots, h_k)$ are stable in the Lyapunov sense. Each perturbed solution tends asymptotically to one of those mentioned above as $t \longrightarrow +\infty$. The theorem has been proved.

For solutions of family (2), the proof of Theorem 1 leads to the sufficient criterion of instability in the Lyapunov sense. It is formulated below.

Theorem 2. *Let conditions* (i) *and* (ii) *of Theorem 1 hold. If the period* ω *of the family of periodic solutions* (2) *is a parameter, then, at sufficiently small values of* $|h_1|, \ldots, |h_k|$, *each solution of family* (2) *is unstable in the Lyapunov sense.*

Obviously, Theorem 1 is valid as well in the case of the periodic solution $x_s = \varphi_s(t)$ ($s = 1, \ldots, n$). This case, which was under study in [3], corresponds to the one-parameter family $x_s = \varphi_s(t + h)$ ($s = 1, \ldots, n$), where h is

the parameter. The case of the family of periodic solutions $x_s = \varphi_s(t, h_1, \ldots, h_k)$ ($s = 1, \ldots, n + k$) was under investigation in [4]. The sufficient conditions of stability in the Lyapunov sense have been established in papers [3, 4]. Theorem 1 shows that the conditions of the Andronov–Vitt theorem and the Malkin theorem are not only sufficient but also necessary.

Theorem 2 is new and can be applied in celestial mechanics [5]. In particular, a theorem formulated below is established with its help.

Theorem 3. *Canonical equations of motion corresponding to the general three-body problem and written in the synodic coordinate system describe a family of periodic motions of an arbitrary period. These motions are unstable in the Lyapunov sense.*

ACKNOWLEDGMENTS

The author is grateful to V.V. Rumyantsev and A.A. Shestakov for attention to this study.

REFERENCES

1. A. M. Lyapunov, *General Problem of Stability of Motion* (Gostekhizdat, Moscow, 1950).
2. B. P. Demidovich, *Lectures on Mathematical Stability Theory* (Nauka, Moscow, 1967).
3. A. Andronov and A. Vitt, Zh. Éksp. Teor. Fiz. **3**, 373 (1933).
4. I. G. Malkin, Prikl. Mat. Mekh. **8**, 327 (1944).
5. E. L. Stiefel and G. Scheifele, *Linear and Regular Celestial Mechanics* (Springer, Berlin, 1971; Nauka, Moscow, 1975).

Translated by Yu. Verevochkin

Doklady Physics, Vol. 45, No. 3, 2000, pp. 93–96. Translated from Doklady Akademii Nauk, Vol. 371, No. 1, 2000, pp. 38–41.

PHYSICS

On a Peculiarity of Structure Formation in Combustion of High-Caloric Metallothermic Compounds under Microgravity Conditions

Academician A. G. Merzhanov, V. N. Sanin, and V. I. Yukhvid

Received November 12, 1999

Gravity strongly affects the combustion of high-caloric metallothermic compounds. In these processes, high-temperature heterogeneous melts composed of mutually insoluble components are produced as the products of combustion. Usually, these melts contain a metallic (heavy) and oxide (lighter) phases. In the gravity field, the phase separation takes place on the macroscopic level (the heavy phase precipitates and the lighter phase rises to the surface) and a two-layer (or multilayer) cast product is eventually formed. This phenomenon was used in investigating the processes of the self-propagating high-temperature synthesis in centrifugal separators, in which the gravity effect of phase separation was enhanced [1–3]. Of no less interest is the opposite formulation of the problem: to study how these processes proceed in the weightless state, i.e., without gravity. Earlier, a marked effect of microgravity on combustion processes and structure formation was noted in combustion of element-containing mixtures [4–7].

In this paper, we present the results of the pioneering experiments on the "liquid-flame" combustion of metallothermic compounds, which were carried out at the orbital space station "Mir".

In the preliminary investigations on the earth, we conducted a search for an initial system for realizing a "liquid" flame under the microgravity conditions. Based on the results of the thermodynamic analysis and experiments, the composition containing 60% of the thermite mixture 3NiO + 5Al and 40% of the mixture of elements Ni + Al was chosen as the model system. The overall scheme of the chemical transformation in this mixture is of the form:

$$3\mathrm{NiO} + \frac{39}{5}\mathrm{Al} + \frac{14}{5}\mathrm{Ni} \longrightarrow \frac{29}{5}\mathrm{NiAl} + \mathrm{Al_2O_3}.$$

The model mixture satisfies the principal requirements of the space "liquid-flame" experiment:

a high temperature (2650 K) is attained in combustion; at this temperature, all the condensed substances (initial, intermediate, and final) are in the liquid-phase state, while the concentration of gaseous products (vapors and suboxides) is low;

the combustion of the mixture proceeds within the steady regime with a low rate (~0.5 cm/s), the substance loss caused by dispersing the melt is less than 1%, and the combustion products (aluminum oxide and nickel aluminide) take the cast form with a distinct separation of layers.

The major set of experiments on realizing the "liquid-flame" combustion under the microgravity conditions at the "Mir" station[1] and the comparative terrestrial experiments were carried out using the setup "Optizon" at the air pressure of 0.4 atm [8]. For the synthesis, we used the powders of NiO, Ni, and Al with the particle sizes less than 10 μm. After mixing, the initial mixtures were pressed in the form of tablets with mass of 4.5 g, 8.5 mm in diameter, and 20 mm in height. The tablets were placed in quartz cups of 13 mm in diameter and 80 mm in height. The tablets were ignited by locally heating the upper face of a tablet employing focused beams from three halogen lamps. Upon completion of the experiments at the "Mir" station, the samples were transported to the earth for investigation. A visual analysis of the combustion products revealed that, under both the microgravity and terrestrial conditions, the metallic and oxide phases were separated. In both cases, the combustion products took the cast form. The comparison between the characteristics of combustion products produced under the microgravity conditions and natural terrestrial conditions showed that they differ only slightly (see table). The X-ray phase analysis has shown that the combustion products obtained both at the "Mir" station and under the terrestrial conditions are identical. In both cases, the metallic phase represents nickel aluminide (NiAl) with the b.c.c. lattice, and the oxide phase is aluminum oxide with the corundum lattice. Thus, we can conclude that the grav-

Institute of Structural Macrokinetics,
Russian Academy of Sciences,
Chernogolovka, Moscow oblast, 142432 Russia

[1] The gravity acceleration at the "Mir" station is $10^{-2}g$, where g is the free fall acceleration.

1028-3358/00/4503-0093$20.00

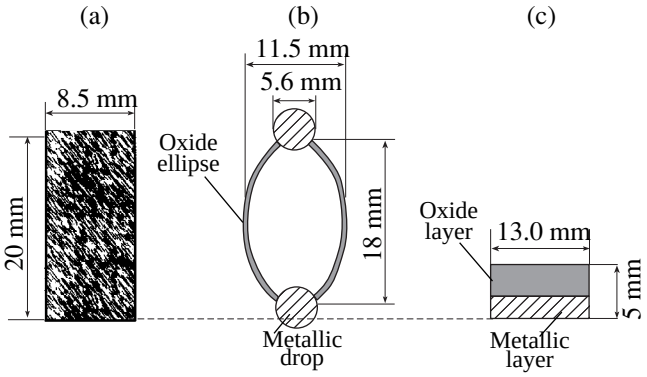

Fig. 1. Effect of microgravity on the macrostructure of cast combustion products: (a) initial tablet; (b) space experiment; and (c) terrestrial experiment.

ity only weakly affects the processes of dispersion, the formation of chemical and phase compositions of the combustion products, and also the completeness of the phase separation between the metallic and oxide phases.

Contrastingly, the macrostructures of the cast products obtained under the space and terrestrial conditions are dramatically different. Under the microgravity conditions, the oxide phase is formed in the shape of a thin-wall shell (a prolate spheroid). At the poles of the shell, metallic particles of spherical form and of approximately equal weight ($m \sim 1.5$ g, Fig 1b) are located. Smaller-sized metallic spherical particles ($m \sim 0.2$–0.3 g) were found in the quartz cup. The total height of the object obtained is approximately equal to the height of the initial tablet. The combustion products obtained under terrestrial conditions were in the form of two dense cylindrical layers with a distinct separation between the metallic and oxide layers (Fig. 1c). The total height of the layers is four times less than the height of the initial sample, and the diameter of the layers is equal to the diameter of the quartz cup.

The microanalysis revealed that the samples obtained under the space conditions are dramatically distinct in the microstructure of the oxide phase and are identical in the microstructure of the metallic phase

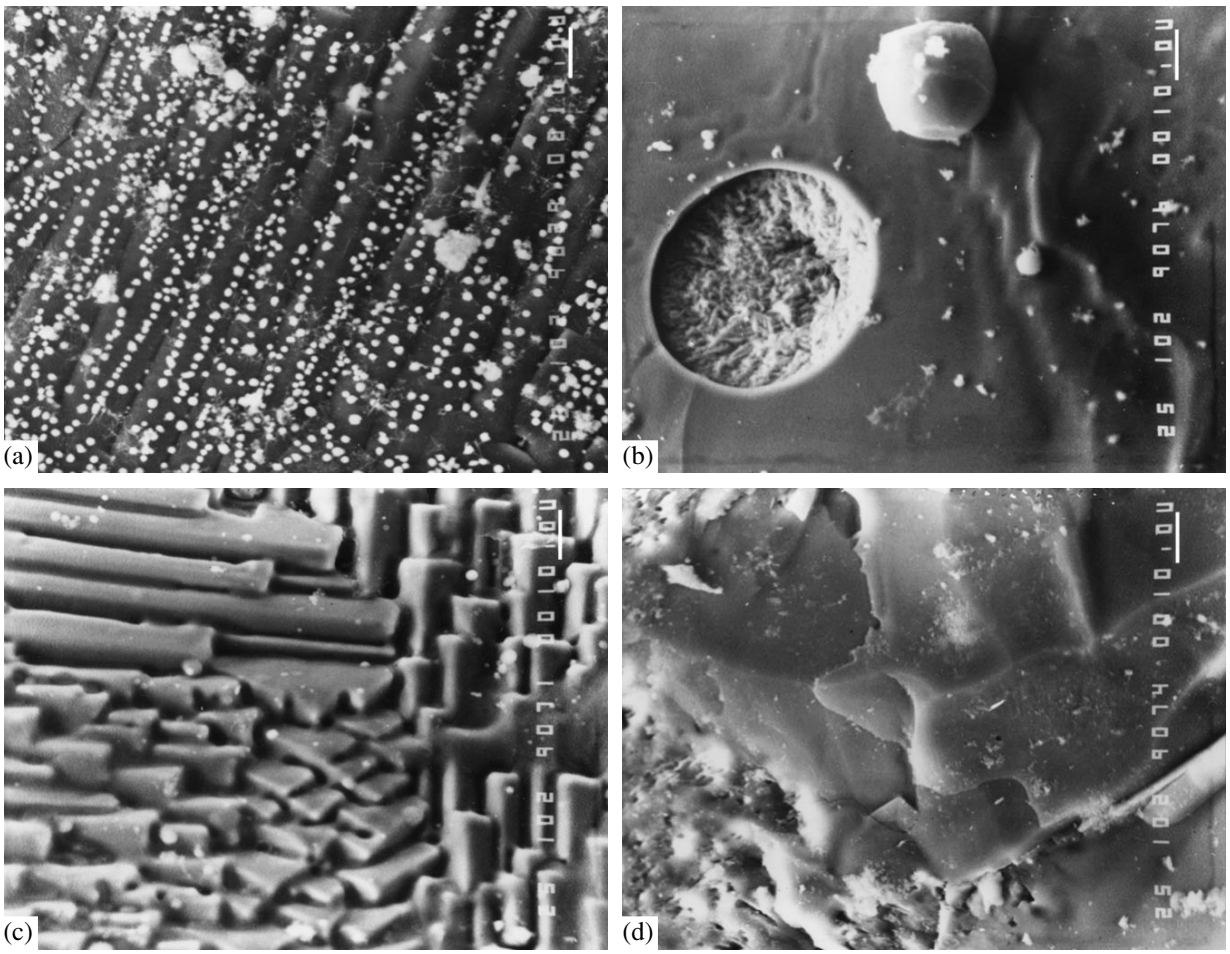

Fig. 2. Effect of microgravity on the microstructure of cast combustion products: (a) and (b) space experiments; (c) and (d) terrestrial experiments; (a) inner surface of the oxide shell; (b) outer surface of the oxide shell; (c) free surface; (d) surface adjacent to the metallic ingot. 400×.

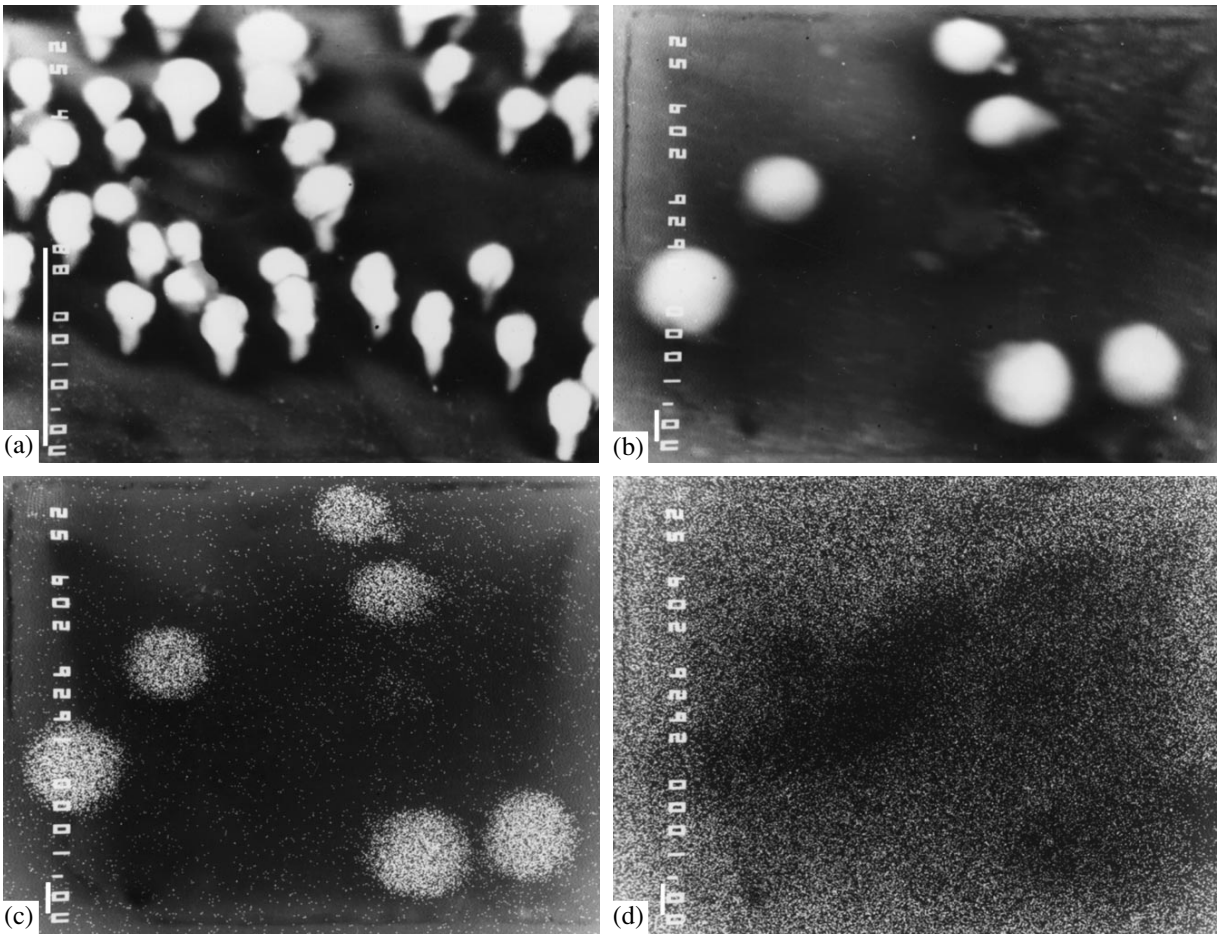

Fig. 3. Distribution of elements in metallic particles at the surface of the oxide shell; (a) and (b) surface element; (c) distribution of Ni; (d) distribution of Al in particles. (a) 4000×; (b), (c), and (d) 6000×.

from that obtained under the terrestrial conditions. Moreover, an appreciable difference between the microstructures of the outer and inner surfaces of the oxide phase of the combustion products (the shell) obtained under the microgravity conditions was revealed (Figs. 2a and 2b). Namely, at the inner surface of the oxide sphere, the alternation of metallic and oxide bands was found, the metallic bands having a discrete structure. The metallic particles forming the rows are mushroom-shaped, contain Ni and Al (Fig. 3), and, according to the X-ray analysis, are intermetallic compounds (NiAl). On the outer surface, there are no metallic "rows," and the major area of this surface is smooth. The analysis of the oxide-film cross section revealed the multitude of channels of the rounded cross section, which came out into the inner cavity of the sphere.

On the surface of the "terrestrial" samples, there are virtually no metallic particles, and the surface has a pronounced relief (Figs. 2c and 2d).

The results obtained enable us to conclude that gravity strongly affects the formation of macrostructure and microstructure of cast combustion products.

It is known that the process of phase separation in the combustion products for the thermite-type systems proceeds in two stages under the terrestrial conditions:

Effect of microgravity on the substance loss in combustion and characteristics of the phase separation

Parameters	Experimental conditions		
	$a = 10^{-2}g$	$a = 1g$	calculated values
Initial mass of a tablet, g	4.5	4.5	4.5
Final mass of products, g	4.0	3.9	4.5
Final mass of the metallic phase, g	3.43	3.30	3.73
Final mass of the oxide phase, g	0.57	0.60	0.77
Depth of dispersion, mass %	11	13	–
Completeness of the metal yield, mass %	92	88	100
Completeness of the oxide yield, mass %	74	78	100

the stage of forming small-sized (primary) drops of the metallic phase caused by the forces of surface (interphase) tension and the stage of precipitating the drops under the action of gravity forces and forming an ingot. In the space experiments, the second stage was absent. Both of these processes, i.e., the formation of the primary drops and the following separation between the metallic and oxide phases, proceed only by the action of the forces of interphase tension without participation of the gravity forces. A whimsical shape of the space products is associated with a weak gassing. Under the terrestrial conditions, the gravity ejects rapidly the gas bubbles from the melt. Under the space conditions, a gas inflates the liquid product and it forms a large bubble.

ACKNOWLEDGMENTS

We thank V.P. Nikitskiĭ (Moscow Scientific and Technical Center for useful loads of space objects) for the support of this work and interest, the astronauts T.A. Musabaev and N.M. Budarin for the realization of these experiments on self-propagating high-temperature synthesis at the orbital "Mir" station, A.I. Ivanov, S.F. Savin, E.V. Markov, V.Yu. Antropov, and A.E. Sychev for the assistance in the realization of this work.

REFERENCES

1. A. G. Merzhanov, V. I. Yukhvid, and I. P. Borovinskaya, Dokl. Akad. Nauk SSSR **255**, 120 (1980).
2. A. G. Merzhanov, Combust. Sci. and Tech. **98**, 307 (1994).
3. A. G. Merzhanov and V. I. Yukhvid, in *Proceedings of the First USA–Japanese Workshop on Combustion Synthesis*, Tsukuba, Japan, 1990 (Tsukuba, 1990), p. 1.
4. A. S. Shteĭnberg, V. A. Shcherbakov, V. V. Martynov, *et al.*, Dokl. Akad. Nauk SSSR **318**, 337 (1991) [Sov. Phys.–Dokl. **36**, 385 (1991)].
5. V. I. Yukhvid, S. L. Silyakov, V. N. Sanin, *et al.*, in *Proceedings of the Joint X European and V Russian Symposiums on Physical Science in Microgravity*, St. Petersburg, Russia, 1997 (St. Petersburg, 1997), p. 397.
6. A. G. Merzhanov, A. S. Rogachev, and A. E. Sychev, Dokl. Akad. Nauk **362**, 217 (1998).
7. A. G. Merzhanov, A. S. Rogachev, V. N. Sanin, *et al.*, J. Jap. Soc. Micrograv. Appl., Supl. II **15**, 550 (1998).
8. Yu. N. Dyakov, E. V. Markov, A. Z. Loobushkin, *et al.*, in *Proceedings of the AIAA/IKI Microgravity Science Symposium*, Moscow, Russia, 1991 (Moscow, 1991), p. 338.

Translated by V. Bukhanov

Doklady Physics, Vol. 45, No. 3, 2000, pp. 97–100. Translated from Doklady Akademii Nauk, Vol. 371, No. 1, 2000, pp. 42–44.

TECHNICAL PHYSICS

Approximation of a Given Function by Integral Functions of the Exponential Type

E. G. Zelkin*, V. F. Kravchenko*, Corresponding Member of the RAS V. I. Pustovoĭt*, and V. V. Timoshenko**

Received July 22, 1999

One of the central problems in the theory of antenna synthesis is the problem of approximating a given directivity pattern by integral functions of exponential type, i.e., by functions related to the class of W_σ functions [1]. In fact, if a given directivity pattern belongs to this class, then there exists an exact solution to the synthesis problem. As is well known [2], the desired directivity pattern for antennas does not belong to this class. Thus, these approximating functions are determined by requirements of practice and can acquire various forms. In this case, the synthesis problem has no exact solution, and a question arises on approximating with a predetermined accuracy a given directivity pattern by functions belonging to the class of W_σ functions.

The statement of the problem. The essence of the approximation method proposed in [2] is the following. The given directivity pattern is approximated by a polynomial $P_k(z)$ of a reasonably high degree. According to the Weĭerstrass theorem, this procedure can be realized with an arbitrary predetermined accuracy. Furthermore, the polynomial obtained is multiplied by an auxiliary function $U_m(z)$ having the following properties:

(I) $U_m(z)$ belongs to the class of W_σ functions;

(II) As $z \longrightarrow \infty$, the function $U_m(z)$ on the real axis has an infinitesimally small value on the order of $o(1/z^m)$, where $m > k$;

(III) In the segment where a directivity pattern is given, the function $U_m(z)$ tends to unity with increasing m, i.e., for any ε_1 there exists a number m, such that $|1 - U_m(z)| < \varepsilon_1$ in the domain $-L/\lambda \le z \le L/\lambda$, where L and λ are the antenna length and wavelength, respectively.

The product $P_k(z)U_m(z)$ belongs to the class of W_σ functions, and, consequently, there exists an amplitude-phase distribution of currents, which depends on the antenna aperture and provides the given directivity pattern.

Indeed, by virtue of the validity of the inequality $|R(z) - P_k(z)| < \varepsilon_2$,

$$\begin{aligned}|R(z) - P_k(z)U_m(z)| &\le |R(z) - R(z)U_m(z)| \\ &+ |R(z)U_m(z) - P_k(z)U_m(z)| < |R(z)|\varepsilon_1 + |U_m(z)|\varepsilon_2.\end{aligned} \tag{1}$$

The conditions $|R(z)| \le 1$ and $|U_m(z)| \le 1$ are satisfied for arbitrary m in the segment $-L/\lambda \le z \le L/\lambda$, and, consequently,

$$|R(z) - P_k(z)U_m(z)| \le \varepsilon_1 + \varepsilon_2, \quad m > k. \tag{2}$$

Similar reasonings are also applicable in the case when trigonometric polynomials $T_k(z)$ are used as approximating functions. Then, the directivity patterns obtained belong to the class of W_σ functions. They are realizable and can be represented in the form of the Kotel'nikov series [2]

$$R_s(z) = \sum_m R_s(m)S(z - m), \tag{3}$$

where

$$\begin{aligned}R_s &= P_k(z)U_m(z), \\ S(z) &= \frac{\sin(\sigma z)}{\sigma z}, \\ z_n &= \frac{\pi n}{\sigma}.\end{aligned} \tag{4}$$

As the auxiliary function $U_m(z)$, it was proposed in [2] a function that represents the Fourier transform of a cosine function of the mth power:

$$U_m(z) = \frac{1}{2\pi}\int_{-\pi}^{\pi} e^{izy}\left[\frac{\Gamma^2(m/2 + 1)}{m!}\left(2\cos\frac{y}{2}\right)^m\right]dy. \tag{5}$$

* *Institute of Radio Engineering and Electronics, Russian Academy of Sciences, Mokhovaya ul. 11, Moscow, 103907 Russia*

** *Central Design Bureau of Unique Instrumentation, Russian Academy of Sciences, ul. Butlerova 15, Moscow, 117342 Russia*

1028-3358/00/4503-0097$20.00

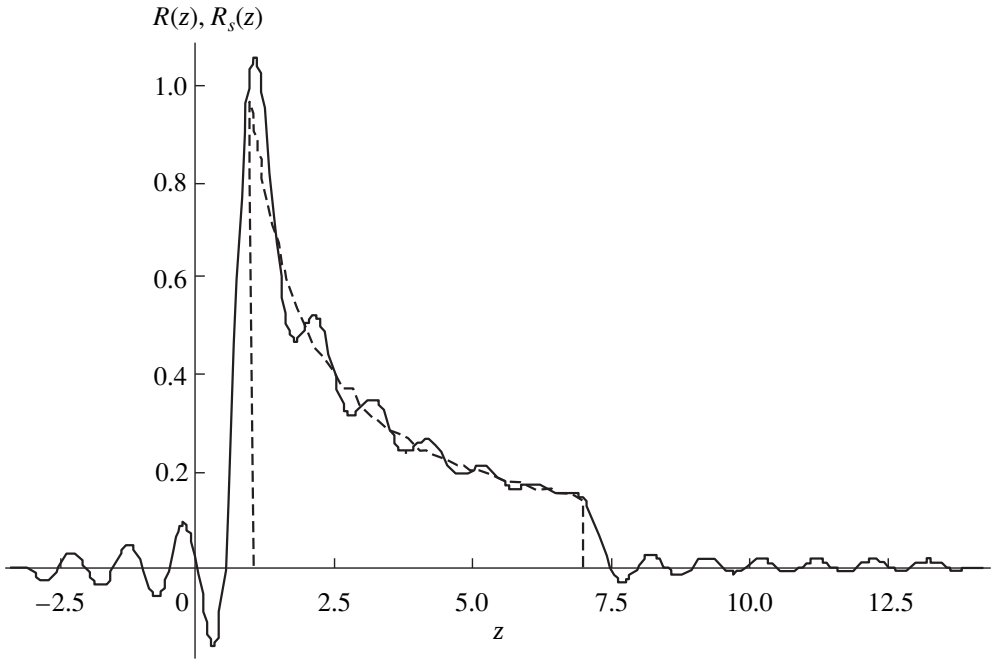

Fig. 1.

Here, $\Gamma(\alpha)$ is the gamma function. For even and odd m,

$$U_m(z) = \frac{\sin\pi z}{\pi z\prod_{p=1}^{m}\left(1-\frac{z^2}{p^2}\right)}, \quad (6)$$

and

$$U_m(z) = \frac{\cos\pi z}{\prod_{p=1}^{m}\left(1-\left(\frac{2z}{2p+1}\right)^2\right)}, \quad (7)$$

respectively. Both these functions belong to the class of W_π functions. They have a maximum equal to unity at the point $z = 0$. The first zero is located at the points $z = m/2 + 1$. For all points at which $z = n$ and $n \le m$, the equality

$$U_m(n) = \frac{(m!)^2}{(m+n)!(m-n)!} \quad (8)$$

is valid. At the points $z = n$ and $n > m$, $U_m(n) = 0$. By the appropriate choice of m, we can approach the function $U_m(z)$ infinitely close to unity in the given interval, and approximate the given directivity pattern with an arbitrary predetermined accuracy [see (2)]. We note that the use of the function $U_m(z)$ as an auxiliary one in practical calculations is not necessarily advantageous. In the cases when the ratio L/λ is large, the degree of the polynomial $P_k(z)$ must be high enough. However, due to the fact that $m > k$, the function $U_m(z)$ will tend to zero slowly outside the segment $L/\lambda \le |z| \le m$. This leads to the appearance of lateral lobes that can be successfully suppressed by the theory of atomic functions.

Atomic functions. As is well known, there exists a numerous family of atomic functions [3]. The simplest of them denoted as up(y) obeys the following differential equation:

$$\frac{d\,\mathrm{up}(y)}{dt} = 2\mathrm{up}(2y+1) - 2\mathrm{up}(2y-1). \quad (9)$$

The Fourier transform of the function up(y) has the form

$$Up(z) = \frac{1}{2\pi}\int_{-\infty}^{\infty} e^{iyz}\mathrm{up}(y)dy = \prod_{p=1}^{\infty}\frac{\sin z\times 2^{-p}}{z\times 2^{-p}}. \quad (10)$$

The function up(y) is infinitely differentiable, finite, and obeys the following properties:

$$\text{(a)}\ \ 0 \le \mathrm{up}(y) \le 1, \quad \mathrm{up}(-y) = \mathrm{up}(y),$$
$$\text{(b)}\ \ \sum_{k=-\infty}^{\infty}\mathrm{up}(y-k) \equiv 1. \quad (11)$$

This function was employed as an auxiliary one for the approximation of a given directivity pattern [3, 4]. After this approximation has been realized, the directivity pattern obtained is the minimum one outside the segment $-L/\lambda \le z \le L/\lambda$. In [3], the atomic function $\Xi_n(y)$

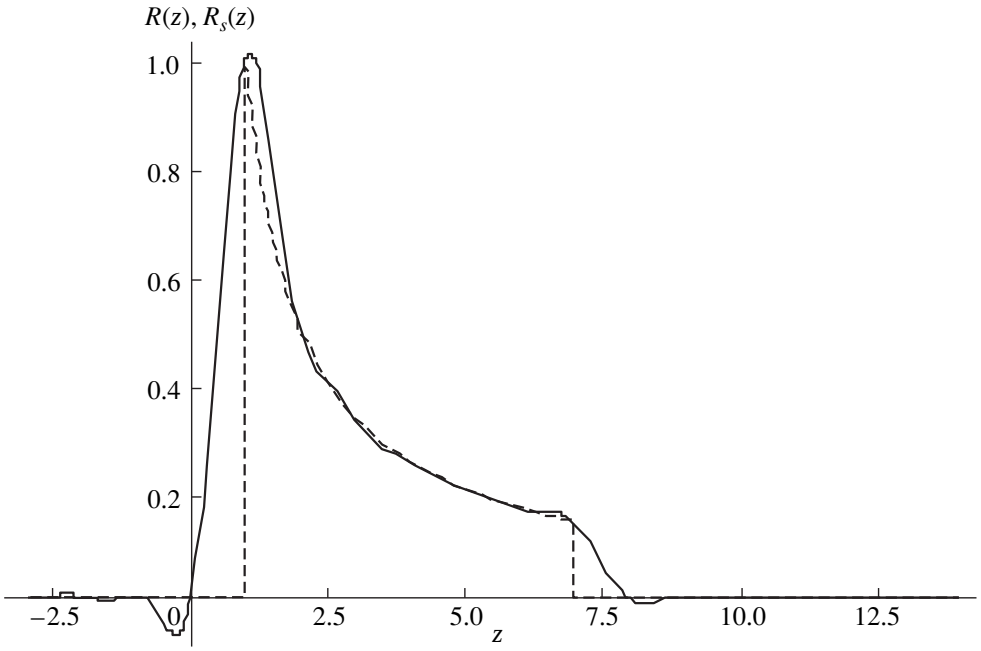

Fig. 2.

was used while solving the synthesis problem. The Fourier transform of this function has the form

$$K_n(z) = \prod_{p=1}^{\infty}\left[\frac{\sin z(n+1)^{-p}}{z(n+1)^{-p}}\right]^n. \qquad (12)$$

For $n = 1$, $\Xi_1(y) = \mathrm{up}(y)$. At the present time, the following approximating functions and corresponding distributions $f_s(y)$ of the electric current (field) along the antenna length are studied:

(I) Approximation by trigonometric polynomials:

$$R_s(z) = K_n(\alpha z)\sum_{m=-\beta(1-\alpha)/\alpha}^{\beta(1-\alpha)/\alpha} a_m e^{-i\beta z m}, \qquad (13)$$

$$f_s(y) = \sum_{m=-\beta(1-\alpha)/\alpha}^{\beta(1-\alpha)/\alpha} a_m \Xi_n\left(\frac{y-\beta m}{\alpha}\right). \qquad (14)$$

(II) Approximation by shifts of the functions $K_n(z)$:

$$R_s(z) = \sum_m a_m K_n(\alpha(z-\beta m)), \qquad (15)$$

$$f_s(z) = \Xi_n\left(\frac{z}{\alpha}\right)\sum_m a_m e^{-i\beta y m}. \qquad (16)$$

(III) Approximation by polynomials:

$$R_s(z) = K_n(\alpha z)\sum_{m=0}^{k} a_m z^m, \qquad (17)$$

$$f_s(y) = \alpha\sum_{m=0}^{k}\left(-\frac{i}{\alpha}\right)^m a_m \Xi_n^{(m)}\left(\frac{y}{\alpha}\right). \qquad (18)$$

The choice of the parameters α, β and a_n for these functions is determined by the accepted approximation methods (the mean-square, uniform, and pointwise approximations) [3].

Numerical experiment. Numerical calculations by the methods proposed and substantiated above were conducted for a cosecant directivity pattern under the following conditions:

$$R(z) = \begin{cases} 0, & z \notin (1, 7) \\ \mathrm{cosec}(z), & z \in (1, 7). \end{cases} \qquad (19)$$

The plots for directivity pattern (19) (dashed line) and directivity pattern synthesized by the Woodward method [4] (solid line) are shown in Fig. 1 ($L/\lambda = 3\pi$). The directivity pattern plotted by the method of atomic functions [see formulas (15), (16)] with the parameters $n = 1$, $\alpha = 2\pi$, $\beta = 1$, $a_m = R(m)$ are shown in Fig. 2. The comparison and physical analysis of the results

obtained have shown that the more exact approximation of directivity patterns is attained owing to unique properties of the atomic function [3]. For example, in the non-zero segments of $R(z)$, oscillations of the function $R_s(z)$ (15) and its side lobes are essentially suppressed.

Thus, the method for approximating directivity patterns by integral functions of the exponential type is substantiated by the theory of atomic functions. Such an approach appears to be rather promising in analysis and synthesis of a new class of radiating systems.

REFERENCES

1. N. I. Akhieser, *Lectures on the Approximation Theory* (Nauka, Moscow, 1965).
2. E. G. Zelkin and V. G. Sokolov, *Methods for Antenna Synthesis* (Sovetskoe Radio, Moscow, 1980).
3. V. F. Kravchenko., V. I. Pustovoĭt, and V. V. Timoshenko, Dokl. Akad. Nauk **368**, 184 (1999) [Dokl. Phys. **44**, 610 (1999)].
4. V. F. Kravchenko, Electromagn. Waves and Electron. Systems **3**, 40 (1998).

Translated by V. Devitsyn